Title

The medial entorhinal cortex is necessary for temporal organization of hippocampal neuronal activity.

Journal

Nature neuroscience, 18(8)

ISSN

1097-6256

Authors

Schlesiger, Magdalene I
Cannova, Christopher C
Boublil, Brittney L
et al.

Publication Date

2015-08-01

DOI

10.1038/nn.4056

Peer reviewed

HHS Public Access

Author manuscript

Nat Neurosci. Author manuscript; available in PMC 2016 February 01.

Published in final edited form as:

Nat Neurosci. 2015 August ; 18(8): 1123–1132. doi:10.1038/nn.4056.

THE MEDIAL ENTORHINAL CORTEX IS NECESSARY FOR TEMPORAL ORGANIZATION OF HIPPOCAMPAL NEURONAL ACTIVITY

Magdalene I. Schlesiger[1,2,6], **Christopher C. Cannova**[1,6], **Brittney L. Boublil**[1], **Jena B. Hales**[3], **Emily A. Mankin**[1], **Mark P. Brandon**[1], **Jill K. Leutgeb**[1], **Christian Leibold**[4], and **Stefan Leutgeb**[1,5,7]

[1]Neurobiology Section and Center for Neural Circuits and Behavior, University of California, San Diego, La Jolla, California, 92093, U.S.A

[2]Graduate School of Systemic Neurosciences, Ludwig-Maximilians-Universität, Munich, 82152, Planegg, 14 Germany

[3]Department of Psychiatry, School of Medicine, University of California, San Diego, La Jolla, California, 92093, U.S.A

[4]Department Biology II, Ludwig-Maximilians-Universität, Munich, 82152, Planegg, Germany

[5]Kavli Institute for Brain and Mind, University of California, San Diego, La Jolla, California, 92093, U.S.A

Abstract

The superficial layers of the medial entorhinal cortex (MEC) are the major input to the hippocampus. The high proportion of spatially modulated cells, including grid cells and border cells, in these layers suggests that the MEC inputs to the hippocampus are critical for the representation of space in the hippocampus. However, selective manipulations of the MEC do not completely abolish hippocampal spatial firing. To therefore determine whether other hippocampal firing characteristics depend more critically on MEC inputs, we recorded from hippocampal CA1 cells in rats with MEC lesions. Strikingly, theta phase precession was substantially disrupted, even during periods of stable spatial firing. Our findings indicate that MEC inputs to the hippocampus are required for the temporal organization of hippocampal firing patterns and suggest that cognitive functions that depend on precise neuronal sequences within the hippocampal theta cycle are particularly dependent on the MEC.

[7]Corresponding author. Address: 9500 Gilman Dr., MC 0357, University of California, San Diego, La Jolla, CA 92093. sleutgeb@ucsd.edu 23.

[6]These authors contributed equally to this work.

AUTHOR CONTRIBUTIONS

M.I.S., S.L., and J.K.L designed experiments, M.I.S., J.B.H, and S.L performed surgeries, M.I.S. and B.L.B. acquired data, M.P.B provided data, C.C.C., M.I.S., J.B.H., E.A.M., C.L., and S.L. performed analysis, M.I.S., C.C.C, J.K.L., C.L., and S.L wrote the manuscript.

COMPETING FINANCIAL INTERESTS

The authors declare no competing financial interests.

The high proportion of grid cells and of other cell types with spatial and directional firing patterns in the medial entorhinal cortex (MEC) indicates that its microcircuits are specialized for processing spatial information[1–4]. Even though it has been demonstrated that all spatially modulated cell types in the superficial layers of the MEC project to the hippocampus[5], it is still uncertain to what extent the spatial firing of grid cells and other MEC cell types are required for hippocampal spatial firing. In particular, manipulations that are known to selectively disrupt grid patterns have not yet been reported to have major effects on hippocampal spatial firing in familiar environments[6–9]. Furthermore, near complete lesions of the MEC result in broadening, but not in the absence of hippocampal spatial firing fields[10]. These partial effects on hippocampal spatial firing therefore raise the question whether the MEC might have a prominent role in supporting non-spatial hippocampal circuit functions, such as precise temporal firing.

In addition to the presence of a high proportion of cell types which exhibit spatial firing, the MEC is distinct from other inputs to the hippocampus, such as the lateral entorhinal cortex (LEC), in that it exhibits prominent theta (4–12 Hz) oscillations in the local field potential (LFP)[11]. Moreover, similar to hippocampal place cells[12], the spiking of MEC layer II cells occurs at progressively earlier phases of the LFP theta cycle as the animal traverses a spatial firing field[13,14]. As a consequence of this phase precession, the sequence of firing phases across a population of cells within a theta cycle corresponds to the sequence in which their respective spatial firing fields were traversed over many seconds[15–18]. The compression of sequences on the behavioral timescale (seconds) to the timescale at which neurons communicate (tens of milliseconds within a theta cycle) may allow spike-timing-dependent learning rules to take place and thereby facilitate the storage of sequences in synaptic matrices[17,19,20]. Alternatively, it may reflect the retrieval of sequence memories or predictions[9,16,21–23]. In principle, phase precession could also support both storage and retrieval during different phases of the theta cycle[24].

Even though the significance of phase precession is widely recognized, the cellular and circuit mechanisms by which such temporal precision emerges have remained elusive. The finding that phase precession is retained in the MEC while the hippocampus is inactivated suggests that the MEC can generate phase precession independent of the hippocampus[13]. Moreover, predicted rates and theta phases of hippocampal firing reemerge immediately after transient hippocampal inactivation, which suggests that external cortical inputs to the hippocampus can sustain hippocampal phase precession[25,26]. However, these findings do not identify whether firing patterns that are selectively found in the MEC, such as spatially selective, rhythmically modulated, or phase precessing cells, are necessary for hippocampal phase precession or whether any excitatory input to the hippocampus, including nonrhythmic excitatory inputs from the LEC, may be sufficient for reinstantiation. The idea that the excitation does not need to be theta rhythmic to determine firing phase is supported by models that demonstrate that a ramping excitation along with local rhythmic inhibition can result in phase precession[27]. These models, in turn, are supported by the experimental findings that there is a ramp-like increase of the membrane potential within the place field[28] and that a higher firing rate within a hippocampal place field is coupled to an earlier firing phase in behaving animals[29,30].

To determine whether hippocampal phase precession is organized by the neuronal firing patterns of MEC cells or whether input to the hippocampus from other sources can also provide sufficient excitatory drive to result in phase precession, we performed bilateral lesions of MEC and then recorded from hippocampal CA1 cells while rats ran back and forth on a linear track. Based on the observations that lesions of the entorhinal cortex have only a limited effect on hippocampal spatial firing patterns[10,31,32] and that even large lesions of the entorhinal cortex only partially reduce hippocampal oscillations[33,34], we reasoned that spatial and rhythmic firing characteristics would be sufficiently preserved with an MEC lesion such that we could analyze hippocampal phase precession.

RESULTS

Hippocampal firing patterns were only transiently location-selective with MEC lesions

To ask to what extent hippocampal spatial and temporal firing patterns require the MEC, we obtained single-unit and local field potential (LFP) recordings from the hippocampal CA1 area while rats were running along a linear track. After we verified that our lesion included the entire dorsoventral extent of the MEC (Supplementary Fig. 1), we examined the precision of hippocampal spatial firing (Fig. 1a–f and see Supplementary Fig. 2 for additional example cells). Over the duration of an entire recording session (10–20 min), the spatial firing of hippocampal cells was substantially less precise in MEC-lesioned rats (n = 164 fields from 153 cells in 6 rats) compared to controls (n = 51 fields from 50 cells in 4 rats). The average place field size was 61.4 % larger, spatial information was 51.8 % lower, and the peak firing rate was 32.9 % lower (Fig. 1g–i and Supplementary Table 1), while the mean firing rate was not different between groups (Fig. 1j). However, when we inspected each cell's firing from run to run, we observed that the reduced precision of spatial firing in the MEC lesion group was not the result of a sustained broadening of the firing field, but rather emerged from shifting spatial firing fields over the course of the recording session. The spatial instability occurred even though the recording stability in MEC-lesioned rats was not different from control rats (Supplementary Fig. 3). To identify periods of stable spatial firing (PSSF), we used a sliding window method to detect the longest period (at least five consecutive runs) during which cells were active and had a robust mean spatial correlation score ($r > 0.5$) with a probability of less than 5 % ($P < 0.05$) of being obtained from a shuffled spatial distribution (see **Online Methods**). As expected from only including runs during which the cells were active, the average firing rate during PSSFs compared to the entire session increased, although to a similar extent in both the control and MEC lesion group (Fig. 1j). PSSFs from the cells of control rats tended to comprise most runs within a single session, while PSSFs from the cells of MEC-lesioned rats typically consisted of less than a quarter of the runs (median fraction of all runs in PSSF: 0.74 and 0.19, respectively; Fig. 1c,d,k and Supplementary Fig. 2). To address whether the spatial firing characteristics during PSSFs were comparable between control and MEC-lesioned rats, we recalculated the mean field size, spatial information, and peak firing rate using only data collected during PSSFs, and found that there was no longer a significant difference between the control and the MEC lesion group (Fig. 1g–i).

Theta oscillations persisted at a reduced amplitude and frequency with MEC lesions

Before analyzing the temporal coordination of hippocampal cells, we asked to what extent hippocampal LFP theta oscillations were retained in MEC-lesioned rats. To compare LFP theta power between groups, we used the signal from all tetrodes located in the CA1 pyramidal cell layer (Fig. 2a). The theta power in MEC-lesioned rats was reduced by an average of 63.2 % compared to controls (Fig. 2b and Supplementary Table 1). This reduction could not be accounted for by a difference in the running speed between MEC-lesioned rats and controls (Fig. 2b). To confidently calculate theta phase and frequency despite the reduced theta amplitude, we used $1/f$ normalized spectra to select, for each recording session, a tetrode for which the peak theta power was > 3 times the baseline (Fig. 2c and Supplementary Fig. 1). After normalization and selection, theta power no longer significantly differed between sessions of control and MEC-lesioned rats (Fig. 2d; control, 5.2 fold higher than baseline, MEC lesion, 4.2 fold higher than baseline). However, the median LFP theta frequency was reduced by 0.61 Hz in MEC-lesioned compared to control rats (Fig. 2d). We also examined whether the spike timing of single hippocampal cells remained theta rhythmic (Fig. 2e). Although the theta modulation of hippocampal firing was significantly lower in MEC-lesioned rats compared to controls (Fig. 2f and Supplementary Table 1), a substantial proportion of cells remained theta modulated (theta ratio > 5; control: 96.7 %, 29 of 30 cells in 4/4 rats; MEC-lesion: 51.2 %, 21 of 41 cells in 4/5 rats).

For phase precession, the frequency of intracellular theta oscillations and, consequently, the cells' firing frequency is increased with respect to LFP theta during place field traversals[28]. Accordingly, the median firing frequency of control cells was 1.22 Hz higher than the LFP theta frequency within the same recording sessions. In contrast, the firing frequency of theta modulated cells in MEC-lesioned rats was 1.70 Hz lower than in control cells and was no longer consistently higher than the LFP theta frequency (Fig. 2f). We reasoned that the absence of a consistent frequency difference to LFP theta could result in spiking that is phase-locked to LFP theta. Thus, we assessed each cell's theta phase locking via the mean resultant vector length obtained from its spike phase distribution within the theta cycle. Surprisingly, we found that the degree of phase-locking exhibited by MEC-lesioned animals was not higher than in controls, in which the frequency difference of phase precessing cells would preclude phase locking to LFP theta. These results thus suggest that hippocampal cells, although they partially remain theta modulated without MEC inputs, fire neither at a consistent frequency difference nor at a particularly consistent phase with respect to LFP theta. Thus, we next directly examined whether theta phase precession during passes through the cells' place fields was disrupted.

Hippocampal phase precession was substantially diminished by MEC lesions

We analyzed phase precession by measuring the firing phase of each cell's spikes along the distance through the spatial firing field (Fig. 3a–h and see Supplementary Fig. 4 for additional examples). We initially restricted the analysis to fields that were defined for PSSFs because we reasoned that the results would be most directly comparable to control fields that were equally stable and precise (see Fig. 1g–i). When calculating the circular-linear correlation between the firing phase and distance in the field for spikes pooled from all passes through each field (Fig. 3g,h), we found that the slopes of the regression lines

were significant ($P < 0.05$) and negative for most individual control fields (74.2 %), as expected for phase precession. In contrast, the proportion of place fields with significant negative slopes (28.0 %) was substantially lower in MEC-lesioned rats ($\chi^2 = 16.5$, $df = 1$, $P = 5.0 \times 10^{-5}$, chi-square test). Moreover, the average slope was less than zero in controls, while it was not different from zero in MEC-lesioned rats. Furthermore, it was substantially different between control and MEC-lesioned rats (Fig. 3i). We obtained a corresponding pattern of results when either analyzing data from the entire recording session or when restricting the analysis to place fields < 0.6 m (Supplementary Table 2). Taken together, these results indicate that the relation between firing phase and distance through the field was substantially disrupted in the MEC lesion group.

Although the diminished phase precession when pooling spikes over multiple passes could result from the loss of a direct relation between distance and theta phase, phase precession may also be masked by an onset of spiking at variable phases or by a variable rate of precession during individual passes through the field. To test for this possibility, we next analyzed phase precession during single passes through the place field[35] (see Fig. 3e,f) and averaged, for each field, the slopes for all qualifying passes (see **Online Methods**) (Fig. 3j and Supplementary Fig. 4 for additional example passes). Because a small quantity of phase precession may be masked by including passes in which slopes were inaccurately estimated, we also took the average of only the slopes where the circular-linear correlation was significant ($P < 0.05$). The mean field-averaged slope was less than zero in control rats, not different from zero in MEC-lesioned rats, and different between MEC-lesioned and control rats (Fig. 3j). Furthermore, we performed the single-pass analysis for firing fields that were not limited to PSSFs but were smaller than 0.6 m over the entire recording session as well as for fields of any size over the entire recording session (Supplementary Table 2). While the field-averaged slopes were not different from zero when only considering the smaller fields of the MEC-lesioned rats (all slopes: $n = 41$ fields, $P = 0.17$; only significant slopes: $n = 21$ fields, $P = 0.44$, t test), the slopes were significantly negative when not restricting the field size (all slopes: $n = 133$ fields, $P = 0.00021$, t test; only significant slopes: $n = 89$ fields, $P = 0.035$, t test), but nonetheless remained less negative than in controls ($P = 0.0043$, t test). To identify how phase precession may have been more readily detectable when adding passes with less consistent spatial firing, we examined the slopes of individual passes in detail (Supplementary Fig. 5). While the slopes of single passes through control fields were typically distributed within a narrow range around the mean (median standard deviation: 0.35), the slopes of single passes in MEC-lesioned rats were extremely variable (median standard deviation: 0.91, $P = 3.5 \times 10^{-9}$ compared to controls, Mann-Whitney U test) with many individual slopes smaller than −1 (21.1 % compared to 5.9 % in controls). Because it is known that phase precession in control fields does not exceed one theta cycle[12,36], these results are an additional indication that reliable hippocampal phase precession during individual passes through the field is disrupted by MEC lesions.

Spike timing between pairs of overlapping fields was disrupted

Phase precession is thought to provide a mechanism to achieve consistent spike time differences between simultaneously active place cells[15,18]. Theoretically, however, pairs of neurons could still fire at fixed intervals without relation to the LFP theta cycle. To test for

this possibility, we analyzed whether pairs of neurons with overlapping PSSFs (Fig. 4a,b) showed a correlation between the distance between their place fields and the phase difference within a theta cycle of the spike crosscorrelation function (Fig. 4c,d), as previously reported for control cells[18]. Field distance and theta offset exhibit a circular-linear correlation for control pairs (Fig. 4e) but not for pairs from MEC-lesioned rats (Fig. 4f). Our analysis therefore did not reveal evidence that the spike timing relation between pairs of place cells was retained after MEC lesions, and the observed loss of phase precession was therefore coupled with the broader absence of a temporal code.

Theta-phase and instantaneous firing rate were decoupled by the MEC lesions

It has been observed that it is not only the distance within the place field, but also the firing rate within the field that correlates with theta phase[29,30, but see 37]. This raises the possibility that phase precession is a consequence of more fundamental, cellular parameters, such as the level of a cell's excitation, and that these parameters govern the phase advance irrespective of the distance within a place field. We therefore directly tested whether higher instantaneous firing rates (IFR), irrespective of where on the track they occurred, resulted in spiking at earlier theta phases (Fig. 5a,b). To ensure that the comparison would not be confounded by low firing rates in the MEC lesion group, we first confirmed that the IFR of cells of MEC-lesioned rats were at least that observed in controls (Fig. 5c). As previously reported[29,30], theta phase correlated with IFR in control rats. In contrast, we found that the IFR was unrelated to phase in MEC-lesioned rats (Fig. 5d). Furthermore, we found a correlation between the phase-IFR slope and the phase-distance slope for cells from control but not for cells from MEC-lesioned rats (Fig. 5e). This result indicates that, without contribution from MEC, firing at earlier phases is not predicted by higher firing rates.

Phase precession was also disrupted in two-dimensional environments

Phase precession is also observed during random foraging in two-dimensional environments[15,29,38]. Therefore, we also tested the extent of disruption of hippocampal phase precession in the open field. We first confirmed that we could reliably detect phase precession in place cells of control rats in the open field and then tested whether phase precession was retained in MEC-lesioned rats (Fig. 6 and Supplementary Fig. 6 for additional example cells). Because we previously found that place field size in the open field was increased by the MEC lesion[10], we restricted the analysis to only smaller ($< 0.25\ m^2$) place fields (control, $n = 46/51$ fields in 3/3 rats, MEC lesion, $n = 21/45$ place fields in 4/6 rats). However, similar results were also obtained without field size restriction (Supplementary Table 2). Corresponding to the findings on the linear track, we found that phase precession during random foraging in the open field was substantially diminished in MEC-lesioned rats. When pooling the spikes from all passes through each field, the mean slope was negative for control fields, but not different from zero for fields from MEC-lesioned rats, and different between MEC-lesioned and control rats (Fig. 6d). Moreover, the proportion of fields with significant negative slopes ($P < 0.05$, circular-linear correlation) was substantially larger in control rats than in MEC-lesioned rats (76. 1 % and 23.8 %, $\chi^2 = 16.4$, $df = 1$, $P = 5.2 \times 10^{-5}$, chi-square test). We also analyzed single passes and calculated their average slope for each field (see Supplementary Fig. 7 for examples). The mean field-averaged slope was negative in control rats, not different from zero in MEC-lesioned rats,

and differed between fields from control and MEC-lesioned rats (Fig. 6e). Together, these data demonstrate that phase precession on the linear track and in the open field was disrupted by the MEC lesion.

Reduced theta amplitude was not sufficient for fully disrupting phase precession

Because the power of LFP theta and the theta modulation of individual cells was diminished during recordings on the linear track in MEC-lesioned rats (see Fig. 2b,f), our results are consistent with the interpretation that theta amplitudes at control levels are necessary for phase precession. Contrary to this prediction, we found that phase precession was disrupted in the open field while the LFP theta power of MEC-lesioned rats was not different from controls (see Fig. 6a). This suggests that there may not be a direct link between the amplitude of theta power in the CA1 layer and the disruption of phase precession. However, it has been previously reported that the most profound reduction in LFP theta power after entorhinal lesions is not in the CA1 cell layer but rather in the hippocampal fissure[33,34]. To therefore more directly examine whether a reduction in the cells' theta modulation would disrupt phase precession, we analyzed previously published recordings[7] in the open field during which the cells' theta oscillations were as strongly reduced by pharmacological inactivation of the septal area as by the MEC lesion (Fig. 8a and Supplementary Table 4). As previously reported, 10-min recording sessions were performed in a familiar environment before inactivation and at two time points into the inactivation (30 min and 2 h after muscimol infusion). At both time points, we observed a pronounced reduction of the LFP theta power as well as a pronounced reduction of the theta modulation of individual CA1 cells (Fig. 7a). Despite the substantial reduction of LFP theta power, each recording session had at least one tetrode in which LFP theta power was > 1.5 times the $1/f$ baseline and from which the theta phase could thus be accurately estimated (Supplementary Fig. 8). When comparing the timing of place cell firing with respect to LFP theta phase before and during the septal inactivation, we obtained evidence for retained phase precession from both the circular-linear regression precession analysis of pooled spikes (Fig. 7b,c) and from a higher oscillation frequency of the cells compared to LFP theta (Fig. 8). The mean slope of the phase-distance regression line was negative before inactivation and remained negative during two sessions that were conducted during the inactivation (Fig. 7c and Supplementary Table 3). Even though the slopes remained negative, a partial reduction of phase precession was indicated by a reduction in the proportion of fields with significant negative slopes (baseline, 72.6 %; first inactivation session, 40.9 %; second inactivation session, 52.4 %, $\chi^2 = 10.0$, $df = 2$, $P = 0.0069$, chi-square test). The reduction in phase precession by septal inactivation was nonetheless less pronounced than the reduction by the MEC lesion (Fig. 8 and Supplementary Table 4). Phase precession was thus retained to a larger extent in rats with septal inactivation compared to MEC-lesioned rats. This excludes the possibility that a mere reduction in the amplitude of theta oscillations is sufficient to attenuate phase precession as substantially as the MEC lesion and thus supports a more direct role of the MEC for organizing temporal firing in the hippocampus.

When analyzing the slopes of single rather than of pooled passes during septal inactivation, we could detect phase precession during the baseline session before the inactivation (all slopes, $P < 1.0 \times 10^{-5}$, t test; only significant slopes, $P < 9.3 \times 10^{-9}$, sign test compared to

zero) and during the session 2 h into the inactivation session (all slopes, $P < 2.1 \times 10^{-5}$, *t* test; only significant slopes, $P = 0.020$, sign test compared to zero), but not during the session 30 min into the inactivation (all slopes: $P = 0.54$, *t* test; only significant slopes, $P = 0.86$, sign test compared to zero). The inconsistent phase coding in single-pass data is consistent with a recent report of reduced hippocampal sequence coding on a square linear maze during septal inactivation[9]. To explain the discrepancy between the effect size in the analysis of the pooled and single pass data, we reasoned that low amplitude LFP theta oscillations could elicit jitter in the timing of individual spikes or theta-associated bursts while nonetheless leaving the average trend for phase precession intact. In this way, phase precession would remain more readily detectable when spikes from all passes were pooled but not in single passes (Supplemental Fig. 8). To test whether such a dissociation is feasible, we performed simulations in which we applied increasing levels of random jitter to either the spike times or spike phases of baseline data, and observed the degree of jitter at which the mean of the field-averaged single pass and pooled pass slope distributions became statistically indistinguishable from zero. We found that the field-averaged single-pass distribution was more sensitive than the pooled pass distribution to random fluctuations in spike timing or spike phase (Supplementary Fig. 8). Increased variability in spike timing may thus have resulted in phase precession that remained detectable in the pooled passes but not in single passes.

DISCUSSION

The MEC contains cell types with precise spatial and directional firing patterns, such as grid cells, boundary cells, and head-direction cells[2–4]. All of these cell types have been confirmed to project to the hippocampus[5], and are thought to be necessary for spatially and directionally selective hippocampal firing patterns. In addition, MEC cells have a second key specialization compared to other inputs to the hippocampus – they are prominently theta modulated[11,39]. Our recordings from rats during repeated runs along the same path allowed for a detailed analysis of hippocampal spatial and temporal firing patterns without MEC inputs. We found that location-selective firing was retained but typically only over periods on the order of tens of seconds to minutes. Furthermore, most hippocampal cells remained theta modulated, but their preferred firing frequency in the theta range decreased such that it was no longer consistently faster than the LFP theta frequency. The retained spatial firing and theta modulation afforded us the opportunity to ask to what extent the temporal organization of hippocampal firing was preserved during periods when hippocampal cells consistently fired at a discernible location. We found no consistent relation between the firing phase within the theta cycle and the distance through the place field, and the disruption of phase precession by the MEC lesion was more profound than during septal inactivation despite the comparable reduction in the cells' theta oscillations with both manipulations. Our findings therefore demonstrate that the MEC inputs to the hippocampus are necessary for a major component of hippocampal phase precession.

Furthermore, performing phase precession analysis over periods of stable spatial firing did not reveal more phase precession than was observed when including less consistently tuned firing. Our data therefore do not support a strong coupling between the inheritance of spatial tuning by hippocampal cells and the emergence of phase precession. Conversely, a recent

study has shown that phase precession is retained during virtual reality exploration in which consistent spatial firing patterns were no longer detectable[40]. Taken together, these results indicate that spatial firing patterns of hippocampal place cells and the precise temporal organization of spike timing within theta cycles can be decoupled. If the MEC does not support phase precession through the intermediate step of organizing hippocampal spatial firing, the essential role of MEC cells would be to either directly provide faster oscillatory inputs and/or to enable mechanisms within the hippocampus that result in the cells' accelerated oscillation frequency (Supplementary Fig. 9).

Numerous theoretical hypotheses have been proposed to mechanistically explain how theta phase precession might emerge from oscillations in the hippocampus at the cellular and circuit levels[12,21,28–30,41,42]. In particular, it has been suggested that an increasing ramp-like excitatory input to pyramidal cells is sufficient to explain an increasing firing rate within the place field[28] and, in combination with oscillating membrane potentials, an advance of the firing phase[27,29,30,43,44, but see 37]. In our recordings from MEC-lesioned rats, we found substantial LFP theta oscillations in the hippocampal CA1 cell layer, which can be taken as an indication that the rhythmic somatic inhibition of principal cell populations was at least partially retained[34]. In addition, we found that instantaneous firing rates within a theta cycle were no longer related to the phase advance of spiking within the cycle. To the extent that the firing rate within a cell's place field reflects the level of intracellular excitation, our data therefore suggest that excitatory inputs from sources other than MEC do not combine with oscillatory inhibition to result in the phase advance of spiking within a theta cycle.

It has also been proposed that phase precession throughout distinct phases of the theta cycle depends on different classes of local interneurons, including cholecystokinin basket cells for which GABA-release is modulated by local cannabinoid release[45]. Manipulations of cannabinoid receptors reduce phase precession[22], which suggests that intrahippocampal modulation of inhibition contributes to phase precession. Further evidence for an intrahippocampal contribution to phase precession is that theta sequences of hippocampal cells, which are thought to depend on local recurrent connectivity, are particularly disrupted during septal inactivation[9]. Consistent with this finding and the finding that single-pass phase precession is required for theta sequences[46], we also observed the disruption of single-pass phase precession during septal inactivation (see Supplementary Fig. 8). However, the inactivation did not disrupt mechanisms that resulted, on average, in an accelerated spiking of hippocampal cells compared to the LFP. In contrast, MEC lesions reduced the frequency of cell's theta oscillations to a level such that there was no longer a consistent frequency difference between the cells' and the LFP theta oscillations. Our data therefore suggests a necessary role for specifically MEC inputs in generating the accelerated oscillation frequency of single cells compared to the LFP.

Together with the observation that the intracellular membrane potential does not only show a ramp-like excitation but also an increased theta oscillation frequency within the place field[22,28], this raises the question how the faster intracellular oscillations may emerge from MEC inputs. One possibility is that there are already inputs to CA1 dendrites at the theta frequency of phase precessing cells[34]. However, in this case it would be unlikely that the inputs originate from direct projections of MEC layer III to CA1[47] because many layer III

neurons are phase locked to LFP theta rather than exhibiting phase precession[13,14]. The input frequency of the direct MEC projections would thus need to be accelerated by further dendritic computations[43,48–50]. Alternatively, MEC inputs could take effect more indirectly via MEC layer II, dentate gyrus and CA3, resulting in *de novo* generation of phase precession on that pathway. Although speculative, this *de novo* generation could occur either by the activation of recurrent hippocampal circuitry in the dentate/CA3 region[16,21], or by mossy fiber facilitation[42] and inheritance from CA3 to CA1[47]. The possibility that hippocampal phase precession specifically requires phase precession in layer II grid fields[13], which project to the dentate/CA3 region[5], is less likely based on the observation that medial septal inactivation substantially disrupts the spatial firing patterns of grid cells[6,8] while the inactivation only partially reduced phase precession. However, it remains to be determined whether phase precession in grid cells could be affected to a lesser extent by septal manipulations than the spatial grid patterns. Regardless of the specific mechanism, our findings together indicate that a critical function of the MEC is the generation of precise spike timing during hippocampal theta oscillations and that providing excitation to the hippocampus from LEC and/or other cortical input sources is not sufficient for phase precession. Accordingly, cognitive functions for which neuronal sequences within the hippocampal theta cycle are essential are predicted to be particularly impaired after selective MEC lesions.

ONLINE METHODS

Subjects and surgical procedures

The subjects were ten experimentally naïve, male Long–Evans rats weighing approximately 300–400 g. The surgical procedures were performed as previously described[10]. Six rats received NMDA lesions of the medial entorhinal cortex (MEC) and four control rats underwent a sham surgical procedure. Animals were randomly assigned to either the MEC lesion or the control group such that data acquisition for each group was performed throughout the duration of the study. A fourteen-tetrode recording assembly was implanted during the same surgery. Tetrodes were constructed by twisting four 17 μm polyimide-coated platinum-iridium (90 %/10 %) wires, and the electrode tips were plated with platinum to reduce the impedances to 200–300 kΩ at 1 kHz. The tetrodes were arranged into two bundles, with six to eight independently movable tetrodes that were targeted to the hippocampus of each hemisphere (AP: 4.0., ML: ± 2.45, angled laterally towards CA1 recording sites at approximately ML ± 3.0). Following a 1-week recovery period from surgery, rats were food restricted and maintained at ~90 % of free-feeding body weight. Rats were housed individually on a 12 h reversed light/dark cycle, and all behavioral training and recording sessions was performed in the dark phase of the cycle. All experimental procedures were approved by the Institutional Animal Care and Use Committee at the University of California, San Diego. None of the data that were recorded on the linear track have been previously reported. Data that was recorded in the open field in 8 of the 10 rats (3 of 4 controls; 5 of 6 MEC-lesioned) correspond to those in a published study[10] and were reanalyzed here for phase precession. In addition, previously published data from 4 additional Long-Evans rats in which recordings were performed before and during septal inactivation[7] were reanalyzed for phase precession. The surgical, recording, and behavioral

procedures for these rats have previously been described in detail, and their open field recordings closely correspond to those in the MEC lesion group. The two reported inactivation sessions were performed in the familiar room at approximately 30 minutes and 2 hours after the intraseptal muscimol infusion.

Behavioral tasks and recording procedures

Before surgery, rats were pretrained to forage for randomly scattered cereal crumbs in a black rectangular enclosure (1 m × 1 m, 50 cm walls), containing a polarizing cue card (20 cm × 50 cm). The enclosure remained at a constant location in the room. No curtains were used, thereby allowing the rat a clear view of multiple distal background cues such as a light source and surrounding walls. During this phase, rats were trained for 5 days in two daily 10-min sessions. In addition, 2 of 4 control and 4 of 6 MEC-lesioned rats were also pretrained for 10 days on a six-arm radial maze with 85 cm long and 10 cm wide arms, as previously described[51]. After recovery from surgery, training continued in a different room, which contained a black circular enclosure (1 m diameter, 50 cm walls) with a white cue card (20 cm × 50 cm). In the room where training began after surgery, rats were trained for 5–10 days to randomly forage for two to four 10-min sessions per day. In addition, the subset of rats that was pretrained on the 6-arm maze continued to be trained on the six-arm maze for 12–14 days after surgery. During this period, tetrodes were slowly advanced into the CA1 area of the hippocampus. During tetrode advancement and recordings, the signals were preamplified with a unity gain headstage and then recorded with a data acquisition system with 64 digitally programmable differential amplifiers (Neuralynx, Tucson, AZ, USA) as previously described[10]. As expected[52], sharp wave ripples were not diminished by the MEC lesion and could therefore be used to guide electrode advancement into the cell layer in all rats.

Recording began when tetrodes were stably positioned in the CA1 cell layer and when the rats ran continuously throughout each 10-min random foraging session. One electrode in each hemisphere was used to record a reference signal from the cortex. In the open field environment, recordings were performed in up to six sessions per day for at least 6 days. To ensure that each cell was only included in the data analysis once, we only included the data from the first recording session of a day. After the recordings during random foraging in the open field, hippocampal cells were recorded for up to two sessions on the linear track that each lasted 10–20 min. The session with the highest number of runs between the two ends of the track was selected for analysis. Two rats (one control and one MEC lesion) were additionally trained on the linear track for up to forty sessions with up to eight sessions per day. For both track and open field recordings, only cells from the day with the best isolation distance between clusters were included for each tetrode, except when a tetrode was moved and a clearly different set of cells was identified. In addition, we carefully examined the data from rats with different degrees of experience (e.g., training in the six-arm maze, additional training on the track) but found that phase precession was intact in all control rats and disrupted in all MEC-lesioned rats, irrespective of their training history. We therefore combined the data from all control rats and from all MEC-lesioned rats for the analysis of the open field and the linear track data. Data collection and analysis were not performed blind to the conditions of the experiment.

Histology

The brains were prepared to track the hippocampal tetrode locations in cresyl violet stained sections and to quantify the MEC lesion extent in NeuN (1:15000, Chemicon, CloneA60) stained sections with the Cavalieri method, as previously described[10]. The volume of the spared tissue was estimated for the MEC layer II, MEC layer III, MEC deep layers, dorsal parasubiculum, ventral parasubiculum, and hippocampus. Damage to the brain areas other than MEC was not substantial, as previously reported[10].

Data analysis

All data analysis was performed by importing position data, LFP data, and spike data into Matlab and by further processing the data with custom-written software. All Matlab functions that were written by the authors are available upon request.

Spike sorting—Spike sorting was performed manually using the graphical cluster-cutting software MClust (A. D. Redish, http://redishlab.neuroscience.umn.edu/MClust/MClust.html). Well-isolated clusters in the multidimensional parameter space (consisting of waveform amplitudes, the difference between peak and trough of the waveform, and waveform energies) were considered single hippocampal cells. Autocorrelation and cross-correlation functions were used as additional identification criteria. Putative principal cells were distinguished from putative interneurons by spike width and average rate, and only putative principal cells were included in analysis.

Cluster quality and stability—Cluster quality was accessed by calculating the L-ratio and the Mahalanobis (i.e., isolation) distance[53] for each cluster of spikes recorded during running on the linear track. The Mahalanobis distance was calculated using the same spike-features that were used for spike sorting. Recording stability was quantified by dividing the spikes in each cluster into two equal halves, and by calculating the average amplitude for each half. The two halves were then compared by calculating (1) the amplitude difference on the channel with the highest amplitude, (2) the percent change on the channel with the highest amplitude, and (3) the Euclidean distance between the amplitudes on all four channels. These measures were then compared between cells from MEC-lesioned and control rats.

One-dimensional path processing—For each complete session, end-track coordinates corresponding to the reward zone were first removed. Next, trajectories with lateral deviation exceeding 10 cm, indicative of stopping behavior, were excluded. Finally, since one-dimensional spatial firing is known to be directionally selective in control cells, the remaining trajectories were split into left- and right-bound sessions. Only the longitudinal (i.e., x) coordinate was used in subsequent analyses.

Rate map construction—One- and two-dimensional rate maps were constructed by splitting the environment into 5 cm and 5×5 cm^2 bins, respectively, where the rate λ_i assigned to the ith bin was calculated as the total number of spikes in that bin divided by the occupancy time in that bin. One-dimensional rate maps were smoothed using a pseudo-Gaussian kernel with a standard deviation of one bin. Two-dimensional rate maps were

constructed using the "adaptive binning" technique described in ref. 15. To prevent rate inflation due to low occupancy, bins with occupancy time less than 150 ms were assigned rates exclusively via the smoothing procedure.

Spatial information—For each cell, the spatial information[54] was calculated as $I=\sum_i p_i \frac{\lambda_i}{\bar{\lambda}} \log_2 \frac{\lambda_i}{\bar{\lambda}}$, where p_i is the probability of finding the animal in the ith bin, λ_i is the rate assigned to the i^{th} bin and $\bar{\lambda}$ is the average bin rate.

Place field definition and size—Place fields were defined as two or more contiguous bins that met or exceeded 20 % of the peak bin rate for a given cell. Cells with peak bin rate less than 2 Hz were not assigned fields, and cell counts that are reported in the Results only include cells with at least one field and, for the spatial analysis on the linear track (see Fig. 1), and the cells twice for which there were fields in both running direction (linear track, control: 50/82; linear track, MEC-lesioned: 153/170; open field, control: 51/101; open field, MEC-lesioned, 45/254). A field boundary and a contour corresponding to 50 % of the peak bin rate were drawn using Matlab's contourc() function. One- and two-dimensional field sizes were calculated as the length between the beginning and end of the field and the area within the field boundary, respectively.

Passes through a field—Candidate passes through a field were defined as groups of time-contiguous position coordinates that were within the field boundary (see place field definition and size, above) and for which the animal spent at least 200 ms within the 50 % contour. A candidate pass was included in the analysis if its average velocity surpassed 3 cm/s, a minimum of 5 spikes over at least four theta cycles were fired during its duration, and the maximum interspike interval during its duration did not exceed 1 s. Only fields with at least one pass meeting these criteria were included in the phase precession analysis (entire session: control, n = 43 cells, MEC lesion, n = 97 cells; PSSFs: control, n = 30 cells, MEC lesion, n = 41 cells).

Selecting periods of stable spatial firing (PSSF)—Conceptually, we defined a period of stable spatial firing (PSSF) as a period of time where a cell exhibited similar spatial firing over the course of five or more consecutive runs (in one direction) along the linear track. To detect PSSFs quantitatively, we examined the mean pairwise correlation between the rate maps of groups of five or more consecutive runs.

In detail, for each cell in an n-run session, a one-dimensional rate map was constructed for each of the n runs. Let $\boldsymbol{m}_k$ be the rate map corresponding to the k^{th} run. A window $\boldsymbol{M}_{wk} = [\boldsymbol{m}_k \boldsymbol{m}_{k+1} \cdots \boldsymbol{m}_{k+w-1}]$ was defined to be a set of w consecutive rate maps beginning with run k. For each window (w = 5,6, …, n; k = 1,2, …, $k - w + 1$), Pearson's correlation coefficient was calculated for all pairs of constituent rate maps; i.e., $r_{ij} = Corr(\boldsymbol{m}_i, \boldsymbol{m}_j)$, $i \neq j$. The mean correlation coefficient for each window was calculated as $\bar{r}_{wk} = \tanh(\bar{z}_{wk})$, where $\bar{z}_{wk}$ is the empirical mean of the Fisher transformed correlation coefficients $z_{ij} = \operatorname{atanh}(r_{ij})$.

A window was considered to exhibit robust spatial firing if its $\bar{r}_{wk}$ met or exceeded 0.5. Since single passes with fewer than 5 spikes were excluded from subsequent analyses (see

above), such runs were labeled disposable. In addition, since the correlation coefficient is undefined for the 0 vector, runs with no spikes were labeled empty. A window was then considered selectable if it contained at most 30 % disposable runs and no empty runs. If W was the largest window size with a stable, selectable window, we selected as a candidate PSSF the $\boldsymbol{M}_{WK}$ such that $\overline{r}_{WK}=\max_k \overline{r}_{Wk}$.

To assess the significance of the spatial stability, for each run, the spike locations were shifted uniformly (with wrapping) by a random quantity. That is, if $\boldsymbol{x}_k$ is the vector of spike locations for the k^{th} run with the element x_{kj} corresponding to the position of the j^{th} spike, ℓ is the track length, and X is a standard normal random variable, then we took the modified spike locations for the k^{th} run as

$$\boldsymbol{x}_k^*=\boldsymbol{x}_k+\frac{1}{2}\ell X+\begin{cases}\ell, & \forall x_{kj}<-\frac{1}{2}\ell\\ -\ell, & \forall x_{kj}>l(1-\frac{1}{2}X)\\ 0, & otherwise\end{cases}$$

In this way, the temporal organization of spikes within each run as well as the selectability of each window was retained. A null distribution of correlation scores R_W^0 was then obtained by taking the maximum correlation score of all selectable windows of size W from each of 500 independent shuffles. The candidate PSSF $\boldsymbol{M}_{WK}$ was selected for further analysis if $P(R_W^0>\overline{r}_{WK})\leq 0.05$ and rejected otherwise.

LFP tetrode selection—To ensure accurate phase and frequency estimation, LFP oscillations were inspected visually with Neuroview (Neuralynx), and for each session in control and MEC-lesioned rats, a tetrode with a 1/*f*-corrected theta power > 3 (see below) was chosen. For sessions recorded from rats with septal inactivation, a tetrode that retained 1/*f*-corrected theta power > 1.5 after inactivation was selected. For analysis of LFP theta power in the CA1 pyramidal cell layer, the LFP signals from all tetrodes with well-isolated units were used.

LFP theta frequency and relative power—For each tetrode, a time-frequency spectrogram was calculated via the Chronux[55] (www.chronux.org) function mtspecgramc() using a window size and time step of 20 s and 10 s, respectively. The LFP theta frequency was taken as the frequency at maximum power within the 4–12 Hz frequency band of the time-averaged spectrogram. The time-averaged spectrogram $S(f)$ was then 1/*f*-corrected via the normalization

$$\tilde{S}(f)=\frac{1}{f^{\beta_1}e^{\beta_0}}S(f)$$

where β_0 and β_1 are coefficients obtained from the linear regression of log $S(f)$ on log(f). The relative power was then taken as the maximum power of the normalized spectrum within the 4–12Hz frequency band.

Single cell temporal autocorrelations, frequency and theta ratio—For each cell, spike times were binned at a sampling rate of 500 Hz. The temporal autocorrelation between spike times was calculated from the resulting vector. The power spectrum of the temporal autocorrelation was obtained for the frequency band 0–125 Hz via the Chronux function mtspectrumpb() using a padding factor equal to two powers of 2 over the sample size. The single cell frequency was then taken as the frequency of maximum power within 4–12 Hz. The theta ratio was calculated as the power at the single cell frequency over the average power of the spectrum. Cells were included in this analysis if they had at least one place field on the linear track (control, n = 30 cells, MEC lesion, n = 47 cells) and at least one field < 0.25 m^2 in the open field (control, n = 45 cells, MEC lesion, n = 23 cells).

Instantaneous theta phase, firing phase and phase modulation—A 4–12 Hz bandpass filter was applied to the signal from each tetrode selected for phase estimation (see LFP tetrode selection, above). The instantaneous theta phase was obtained from the Hilbert transform of the filtered signal. Spike and LFP timestamps were then used to linearly interpolate firing phase from these values. The degree to which single cell firing was modulated by theta phase was measured by the length $\bar{R}$ of the mean resultant vector obtained for each cell from the resulting distribution of firing phases. The same set of cells as for calculating the temporal autocorrelation was used.

Distance through a field—For each pass, the distance at the k^{th} position coordinate (x_k, y_k) was calculated as

$$d_k = \sum_{i=1}^{k} \sqrt{(x_i - x_{i-1})^2 + (y_i - y_{i-1})^2}$$

where the point (x_0, y_0) corresponds to the coordinate of field entry. d_0 was defined to be 0. The distance at the j^{th} spike $D_j \in [d_k, d_{k+1}]$ occurring at time $t_j \in [t_k, t_{k+1}]$ was linearly interpolated from these values.

Instantaneous firing rate—For each pass, the instantaneous firing rate at the j^{th} spike IFR_j was calculated as the number of spikes in a 250 ms window (approx. two theta cycles) around the time of the j^{th} spike t_j.

Circular-linear regression: General method—The relationship between circular-linear pairs $\{(x_j, \phi_j)\}_{j=1}^{n}$ was checked for consistency with the linear model $\varphi(x) = 2\pi a x + \varphi_0$ by maximizing the mean result vector length $\bar{R}(a)$ of the circular errors between the measured circular variable φ_j and the model predictions $\varphi(x)$:

$$\overline{R}(a) = \sqrt{\left[\frac{1}{n}\sum_{j=1}^{n}\cos(\phi_j - 2\pi a x_j)\right]^2 + \left[\frac{1}{n}\sum_{j=1}^{n}\sin(\phi_j - 2\pi a x_j)\right]^2}$$

$\bar{R}(a)$ does not permit a unique maximum over the whole real line. Thus, we restrict the slopes to the interval $\mathcal{S}$ = (−2 2) cycles per field and denote the slope of the best fit by $a_{\mathcal{S}}=\underset{a\in\mathcal{S}}{\operatorname{argmax}}\bar{R}(a)$. In particular, a maximum obtained at the boundary values indicates that the true maximum of $\bar{R}(a)$ is not in $\mathcal{S}$ = (−2 2) and the slope estimate is therefore not reliable. Hence, slope estimates $a_{\mathcal{S}}$ such that $2 - |a_{\mathcal{S}}| < 0.01$ were excluded from the analysis. The phase offset φ_0 is subsequently estimated by

$$\phi_0=\operatorname{atan2}\frac{\Sigma_j\sin(\phi_j-2\pi a_{\mathcal{S}}x_j)}{\Sigma_j\cos(\phi_j-2\pi a_{\mathcal{S}}x_j)}$$

To assess the significance of the circular-linear correlation, we first calculate the circular-linear correlation coefficient

$$\rho=\frac{\Sigma_j\sin(\phi_j-\bar{\phi})\sin(\theta_j-\bar{\theta})}{\sqrt{\Sigma_j[\sin(\phi_j-\bar{\phi})]^2\Sigma_i[\sin(\theta_i-\bar{\theta})]^2}}$$

where $\theta_k = 2\pi|a_{\mathcal{S}}|x_k$ (*mod* 2π) is the circular transformation of the linear variable, and $\bar{\varphi}$ and $\bar{\theta}$ are the circular means of the φ_k and θ_k, respectively. For large n and uncorrelated Gaussian random phases (the null hypothesis), the scaled correlation is given by

$$z=\rho\sqrt{n\frac{\lambda_{02}\lambda_{20}}{\lambda_{22}}}$$

where

$$\lambda_{ij}=\frac{1}{n}\sum_{k=1}^{n}\sin^i(\phi_k-\bar{\phi})\sin^j(\theta_k-\bar{\theta})$$

Thus, given *z*, we obtain a *p*-value for the correlation from a cumulative standard normal distribution. The test statistic used to derive the significance of a circular-linear correlation is described in Appendix 2.1 (A2.1) of ref.[35] (see also ref.[56]).

Circular-linear regression: Application—Phase-distance slopes were obtained for each pass through a field by performing circular-linear regression[35] on the points $\{(\tilde{D}_j,\phi_j)\}_{j=1}^{n}$, where $\tilde{D}_j=\frac{D_j}{\max_i(D_i)}$ is the pass normalized distance at the j^{th} spike (see above), and φ_j is the theta phase at the j^{th} spike (see above). An identical procedure was used to calculate the phase-distance slope after pooling the $\{(\tilde{D}_j,\phi_j)\}_{j=1}^{n}$ from all passes through a field. *IFR*-phase slopes were obtained similarly using the *IFR* values pooled across each cell normalized by the cell maximum. The regression slope $a_{\mathcal{S}}$ was obtained from one-dimensional numerical maximization of $\bar{R}(a)$ using MATLAB's fminbnd().

Circular-linear regression: Statistical analysis—Of particular relevance to analyzing phase precession is that the test statistic for the regression line is a test against the null hypothesis that the slope of the regression line is zero. Thus, a significant negative correlation may indicate either robust phase precession or Type I error (a false positive), while a nonsignificant negative correlation may indicate either noise (false or random phase precession) or Type II error (a failure to detect phase precession). Reduced phase precession predicts a shift towards a zero-centered distribution of slopes, along with a smaller proportion of significant negative slopes and a higher likelihood for Type II errors. The absence of phase precession predicts a distribution that is centered around zero and that any remaining significant negative slopes are Type I errors. To be sensitive to detecting both reduced phase precession and the absence of phase precession, we inspected the distribution of all fields' slopes as well as the distribution of only the slopes for which the circular-linear regression was significant. For all slopes, we determined whether the distribution was different from zero (one-sample t-test or sign test) and whether distributions differed between groups (two-sample *t* test or Mann Whitney test). For significant negative slopes ($P < 0.05$, circular-linear regression), we tested whether their proportion differed between groups (chi-square test). For distributions that included significant negative and significant positive slopes ($P < 0.05$, circular-linear correlation), we tested whether their mean or median was centered on zero (one-sample t-test or sign test), based on the prediction that a distribution without phase precession would have an approximately equal number of positive and negative significant slopes. For the latter test, it is important to note that it is the distribution between negative and positive slopes that is of interest and not the absolute values of the slopes because the slopes were already selected by the circular-linear regression for their difference from zero before being tested in the second step for their distribution around zero. We nonetheless included this test to be maximally sensitive to any remaining phase precession.

For single passes through a field, it was determined whether the regression line for each pass was significant ($P < 0.05$, circular-linear correlation), and averages were then calculated separately for all passes through the field and for only the significant passes through the field. The averaging per field was used so that fields with a high number of qualifying passed would not be overrepresented. After averaging single passes per field, the statistical tests that were used for the field-averaged slopes corresponded to those that were used for the slopes from pooled passes.

Crosscorrelation analysis of cell pairs—Only pairs of parallel recorded cells went into this analysis where, during overlapping PSSFs, both cells were firing in the same theta cycle. Spike trains of recorded cells were convolved with a Gaussian with 10 ms standard deviation. The convolved spike trains for the relevant pairs were crosscorrelated and the crosscorrelations were filtered in the theta band (6–12 Hz) and Hilbert transformed to determine the theta phase shift with respect to time difference 0. To obtain the crosscorrelation of the place fields the spike positions were convolved with a Gaussian with standard deviation of 3 cm (red lines in Fig. 5c, d). The maximum of the crosscorrelation function corresponded to the distance between the maximal firing rates of the two cells (place field distance).

Jitter simulation—To simulate spike time jitter, an $\mathcal{N}(0, \sigma)$ random variable was added to the timestamp of each individual spike. The corresponding theta phase of each spike was then calculated as described above. To simulate phase-onset jitter, theta-associated bursts (TABs) were empirically defined as sequences of spikes with maximum ISI not exceeding 20 ms. An $\mathcal{N}(0, \sigma)$ random variable was then added to the estimated spike phases of each TAB, such that all spike phases within a TAB were shifted by the same amount. The phases of spikes that did not occur within a TAB were shifted individually by an analogous procedure. For spike time jitter simulations, the value of σ ranged from 0 to 30 ms in 3 ms intervals; for phase-onset jitter simulations, σ ranged from 0 to 25 % of a theta cycle in 2.5 % intervals. One-hundred simulations were performed for a given σ. For each simulation, a field-averaged and pooled pass distribution of firing phase-distance slopes (see above) was obtained and a one-sided *t* test against zero mean was performed. For each σ, the proportion of simulations significantly different from zero was then quantified as the proportion of 100 trials that the null hypothesis was rejected at the 5% level.

Statistical analysis

All statistical tests used were two-sided, and the significance threshold for all tests was $\alpha = 0.05$.

For each sample distribution, a Kolmogorov-Smirnov (KS) test was used to test the null hypothesis that the z-scored sample was derived from a standard normal distribution. If the KS null hypothesis failed rejection, a one-sample *t* test was used to test the sample mean against zero. Otherwise, a sign test was used to test the sample median against zero.

For each between-group comparison, a two-sample *t* test was used to test equality of means only if both sample distributions failed KS test rejection; otherwise, a Mann-Whitney *U* test was used to test the equality of medians. For within-group comparisons between baseline and septal inactivation sessions, a Wilcoxon signed rank test was used to test for equality of medians. Multiple comparisons were corrected for the familywise error rate (FWER) with the Holm-Bonferroni procedure.

Statistical power was assessed by simulating sample distributions under the appropriate alternative hypothesis using the empirical sample size and using bootstrapped estimates of the relevant population parameters as the true parameters. In particular, the power of one- and two-sample *t* tests was assessed by simulating sample distributions derived from a normal distribution with true mean and standard deviation equal to the respective bootstrapped parameters, while the power of Mann-Whitney *U* tests was assessed by bootstrapping values from the sample distribution above and below the bootstrapped estimate of the median with equal probability. The statistical power was then estimated as the proportion of 10,000 simulations where the null hypothesis was correctly rejected using a given test. With the effect size of phase precession in controls and when using sample sizes corresponding to either the control or lesioned groups, we found that the power was > 0.95 for one-sample tests against the null hypothesis that the slope is equal to zero. This indicates that we would likely have rejected the null hypothesis if there were no effect of the MEC lesion. Furthermore, for all two-sample tests that compared phase precession and theta frequency difference between control and MEC-lesion groups, the power was > 0.99 and >

0.92, respectively. We therefore concluded that the sample sizes were sufficiently large to support the main conclusion.

Supplementary Material

Refer to Web version on PubMed Central for supplementary material.

ACKNOWLEDGEMENTS

The authors thank Mandy Wong for technical assistance, Geoff Diehl for recording control data, and Dr. John Lisman for comments on the manuscript. This work was supported by a Boehringer Ingelheim Fonds PhD fellowship, the German Research Association (DFG) under grant LE 2250/5-1, the Ellison Medical Foundation grant AG-NS-0724-10, Walter F. Heiligenberg Professorship, NSF CRCNS grant 1010463, and NIH grants R21 MH100354 and R01 NS086947.

REFERENCES

1. Quirk GJ, Muller RU, Kubie JL, Ranck JB Jr. The positional firing properties of medial entorhinal neurons: description and comparison with hippocampal place cells. J Neurosci. 1992; 12:1945–1963. [PubMed: 1578279]
2. Hafting T, Fyhn M, Molden S, Moser MB, Moser EI. Microstructure of a spatial map in the entorhinal cortex. Nature. 2005; 436:801–806. [PubMed: 15965463]
3. Sargolini F, et al. Conjunctive representation of position, direction, and velocity in entorhinal cortex. Science. 2006; 312:758–762. [PubMed: 16675704]
4. Solstad T, Boccara CN, Kropff E, Moser MB, Moser EI. Representation of geometric borders in the entorhinal cortex. Science. 2008; 322:1865–1868. [PubMed: 19095945]
5. Zhang SJ, et al. Optogenetic dissection of entorhinal-hippocampal functional connectivity. Science. 2013; 340:1232627. [PubMed: 23559255]
6. Brandon MP, et al. Reduction of theta rhythm dissociates grid cell spatial periodicity from directional tuning. Science. 2011; 332:595–599. [PubMed: 21527714]
7. Brandon MP, Koenig J, Leutgeb JK, Leutgeb S. New and distinct hippocampal place codes are generated in a new environment during septal inactivation. Neuron. 2014; 82:789–796. [PubMed: 24853939]
8. Koenig J, Linder AN, Leutgeb JK, Leutgeb S. The spatial periodicity of grid cells is not sustained during reduced theta oscillations. Science. 2011; 332:592–595. [PubMed: 21527713]
9. Wang Y, Romani S, Lustig B, Leonardo A, Pastalkova E. Theta sequences are essential for internally generated hippocampal firing fields. Nat Neurosci. 2014
10. Hales JB, et al. Medial entorhinal cortex lesions only partially disrupt hippocampal place cells and hippocampus-dependent place memory. Cell reports. 2014
11. Deshmukh SS, Yoganarasimha D, Voicu H, Knierim JJ. Theta modulation in the medial and the lateral entorhinal cortices. J Neurophysiol. 2010; 104:994–1006. [PubMed: 20505130]
12. O'Keefe J, Recce ML. Phase relationship between hippocampal place units and the EEG theta rhythm. Hippocampus. 1993; 3:317–330. [PubMed: 8353611]
13. Hafting T, Fyhn M, Bonnevie T, Moser MB, Moser EI. Hippocampus-independent phase precession in entorhinal grid cells. Nature. 2008; 453:1248–1252. [PubMed: 18480753]
14. Mizuseki K, Sirota A, Pastalkova E, Buzsaki G. Theta oscillations provide temporal windows for local circuit computation in the entorhinal-hippocampal loop. Neuron. 2009; 64:267–280. [PubMed: 19874793]
15. Skaggs WE, McNaughton BL, Wilson MA, Barnes CA. Theta phase precession in hippocampal neuronal populations and the compression of temporal sequences. Hippocampus. 1996; 6:149–172. [PubMed: 8797016]
16. Jensen O, Lisman JE. Hippocampal CA3 region predicts memory sequences: accounting for the phase precession of place cells. Learn Mem. 1996; 3:279–287. [PubMed: 10456097]

17. Melamed O, Gerstner W, Maass W, Tsodyks M, Markram H. Coding and learning of behavioral sequences. Trends Neurosci. 2004; 27:11–14. discussion 14–15. [PubMed: 14698603]
18. Dragoi G, Buzsaki G. Temporal encoding of place sequences by hippocampal cell assemblies. Neuron. 2006; 50:145–157. [PubMed: 16600862]
19. Bi G, Poo M. Synaptic modification by correlated activity: Hebb's postulate revisited. Annu Rev Neurosci. 2001; 24:139–166. [PubMed: 11283308]
20. Byrnes S, Burkitt AN, Grayden DB, Meffin H. Learning a sparse code for temporal sequences using STDP and sequence compression. Neural Comput. 2011; 23:2567–2598. [PubMed: 21732857]
21. Tsodyks MV, Skaggs WE, Sejnowski TJ, McNaughton BL. Population dynamics and theta rhythm phase precession of hippocampal place cell firing: A spiking neuron model. Hippocampus. 1996; 6:271–280. [PubMed: 8841826]
22. Robbe D, Buzsaki G. Alteration of theta timescale dynamics of hippocampal place cells by a cannabinoid is associated with memory impairment. J Neurosci. 2009; 29:12597–12605. [PubMed: 19812334]
23. Gupta AS, van der Meer MA, Touretzky DS, Redish AD. Segmentation of spatial experience by hippocampal theta sequences. Nat Neurosci. 2012; 15:1032–1039. [PubMed: 22706269]
24. Hasselmo ME, Bodelon C, Wyble BP. A proposed function for hippocampal theta rhythm: separate phases of encoding and retrieval enhance reversal of prior learning. Neural Comput. 2002; 14:793–817. [PubMed: 11936962]
25. Zugaro MB, Monconduit L, Buzsaki G. Spike phase precession persists after transient intrahippocampal perturbation. Nat Neurosci. 2005; 8:67–71. [PubMed: 15592464]
26. Moser EI, et al. A test of the reverberatory activity hypothesis for hippocampal 'place' cells. Neuroscience. 2005; 130:519–526. [PubMed: 15664708]
27. Mehta MR. Neuronal dynamics of predictive coding. Neuroscientist. 2001; 7:490–495. [PubMed: 11765126]
28. Harvey CD, Collman F, Dombeck DA, Tank DW. Intracellular dynamics of hippocampal place cells during virtual navigation. Nature. 2009; 461:941–946. [PubMed: 19829374]
29. Harris KD, et al. Spike train dynamics predicts theta-related phase precession in hippocampal pyramidal cells. Nature. 2002; 417:738–741. [PubMed: 12066184]
30. Mehta MR, Lee AK, Wilson MA. Role of experience and oscillations in transforming a rate code into a temporal code. Nature. 2002; 417:741–746. [PubMed: 12066185]
31. Miller VM, Best PJ. Spatial correlates of hippocampal unit activity are altered by lesions of the fornix and endorhinal cortex. Brain Res. 1980; 194:311–323. [PubMed: 7388617]
32. Van Cauter T, Poucet B, Save E. Unstable CA1 place cell representation in rats with entorhinal cortex lesions. Eur J Neurosci. 2008; 27:1933–1946. [PubMed: 18412614]
33. Ylinen A, et al. Intracellular correlates of hippocampal theta rhythm in identified pyramidal cells, granule cells, and basket cells. Hippocampus. 1995; 5:78–90. [PubMed: 7787949]
34. Kamondi A, Acsady L, Wang XJ, Buzsaki G. Theta oscillations in somata and dendrites of hippocampal pyramidal cells in vivo: activity-dependent phase-precession of action potentials. Hippocampus. 1998; 8:244–261. [PubMed: 9662139]
35. Kempter R, Leibold C, Buzsaki G, Diba K, Schmidt R. Quantifying circular-linear associations: hippocampal phase precession. J Neurosci Methods. 2012; 207:113–124. [PubMed: 22487609]
36. Maurer AP, Cowen SL, Burke SN, Barnes CA, McNaughton BL. Organization of hippocampal cell assemblies based on theta phase precession. Hippocampus. 2006; 16:785–794. [PubMed: 16921501]
37. Huxter J, Burgess N, O'Keefe J. Independent rate and temporal coding in hippocampal pyramidal cells. Nature. 2003; 425:828–832. [PubMed: 14574410]
38. Huxter JR, Senior TJ, Allen K, Csicsvari J. Theta phase-specific codes for two-dimensional position, trajectory and heading in the hippocampus. Nat Neurosci. 2008; 11:587–594. [PubMed: 18425124]
39. Hargreaves EL, Rao G, Lee I, Knierim JJ. Major dissociation between medial and lateral entorhinal input to dorsal hippocampus. Science. 2005; 308:1792–1794. [PubMed: 15961670]

40. Aghajan ZM, et al. Impaired spatial selectivity and intact phase precession in two-dimensional virtual reality. Nat Neurosci. 2015; 18:121–128. [PubMed: 25420065]
41. Lengyel M, Szatmary Z, Erdi P. Dynamically detuned oscillations account for the coupled rate and temporal code of place cell firing. Hippocampus. 2003; 13:700–714. [PubMed: 12962315]
42. Thurley K, Leibold C, Gundlfinger A, Schmitz D, Kempter R. Phase precession through synaptic facilitation. Neural Comput. 2008; 20:1285–1324. [PubMed: 18085985]
43. Magee JC. Dendritic mechanisms of phase precession in hippocampal CA1 pyramidal neurons. J Neurophysiol. 2001; 86:528–532. [PubMed: 11431530]
44. Ekstrom AD, Meltzer J, McNaughton BL, Barnes CA. NMDA receptor antagonism blocks experience-dependent expansion of hippocampal "place fields". Neuron. 2001; 31:631–638. [PubMed: 11545721]
45. Klausberger T, et al. Complementary roles of cholecystokinin- and parvalbumin-expressing GABAergic neurons in hippocampal network oscillations. J Neurosci. 2005; 25:9782–9793. [PubMed: 16237182]
46. Feng T, Silva D, Foster DJ. Dissociation between the Experience-Dependent Development of Hippocampal Theta Sequences and Single-Trial Phase Precession. J Neurosci. 2015; 35:4890–4902. [PubMed: 25810520]
47. Jaramillo J, Schmidt R, Kempter R. Modeling inheritance of phase precession in the hippocampal formation. J Neurosci. 2014; 34:7715–7731. [PubMed: 24872575]
48. Harris KD, Hirase H, Leinekugel X, Henze DA, Buzsaki G. Temporal interaction between single spikes and complex spike bursts in hippocampal pyramidal cells. Neuron. 2001; 32:141–149. [PubMed: 11604145]
49. Chance FS. Hippocampal phase precession from dual input components. J Neurosci. 2012; 32:16693a–16703a. [PubMed: 23175823]
50. Leung LSA. model of intracellular theta phase precession dependent on intrinsic subthreshold membrane currents. J Neurosci. 2011; 31:12282–12296. [PubMed: 21865471]
51. Schlesiger MI, et al. Hippocampal activation during the recall of remote spatial memories in radial maze tasks. Neurobiol Learn Mem. 2013; 106:324–333. [PubMed: 23742919]
52. Bragin A, Jando G, Nadasdy Z, van Landeghem M, Buzsaki G. Dentate EEG spikes and associated interneuronal population bursts in the hippocampal hilar region of the rat. J Neurophysiol. 1995; 73:1691–1705. [PubMed: 7643175]
53. Schmitzer-Torbert N, Jackson J, Henze D, Harris K, Redish AD. Quantitative measures of cluster quality for use in extracellular recordings. Neuroscience. 2005; 131:1–11. [PubMed: 15680687]
54. Skaggs, WE.; McNaughton, BL.; Gothard, KM.; Markus, EJ. An information-theoretic approach to deciphering the hippocampal code. In: Hanson, SJ.; Giles, CL.; Cowan, JD., editors. Advances in Neural Information Processing Systems 5. San Mateo, CA: Morgan Kaufmann; 1993. p. 1030-1037.
55. Bokil H, Andrews P, Kulkarni JE, Mehta S, Mitra PP. Chronux: a platform for analyzing neural signals. J Neurosci Methods. 2010; 192:146–151. [PubMed: 20637804]
56. Jammalamadaka, SR.; SenGupta, A. Topics in circular statistics. Singapore: World Scientific; 2001.

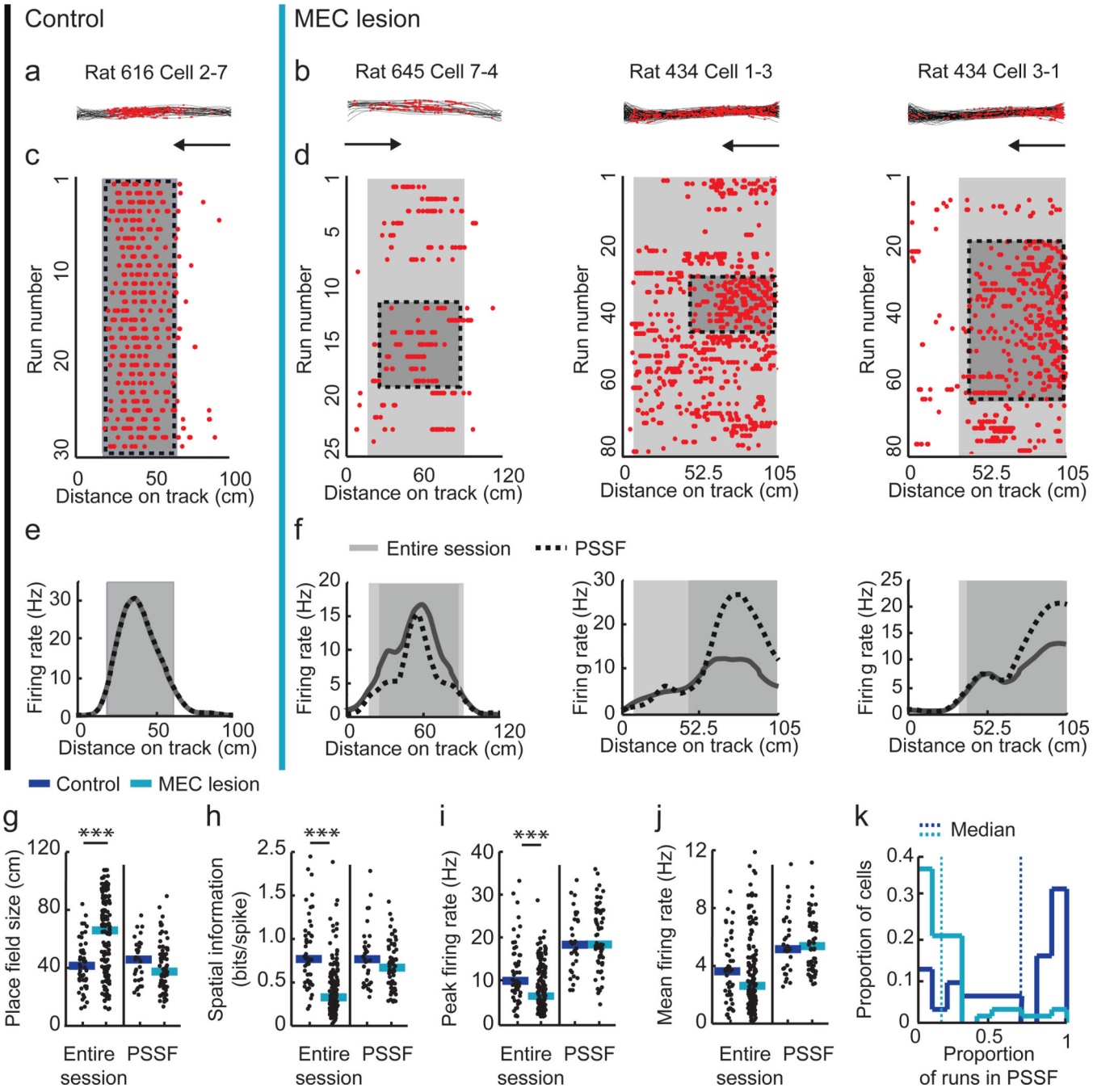

Figure 1. Hippocampal firing patterns were only transiently location selective in MEC-lesioned rats

Each column is data from one hippocampal cell during running in one direction (indicated by arrow) on the linear track (control, black vertical line; MEC lesion, blue vertical line). The cell numbers (e.g., 2–7) include the tetrode and cell identification. (**a,b**) Trajectories (black lines) with spike locations (red dots). Turns were excluded from the analysis and are not shown. (**c,d**) Raster plots with the spike locations during each run. (**e,f**) Rate versus distance on the linear track. In **c**–**f**, place fields for the entire recording session are marked by the entire shaded area and place fields for the period of stable spatial firing (PSSF; see

Online Methods) are marked by the darker shaded area. (**g**–**j**) Spatial firing characteristics during the entire session (control, $n = 51$ fields from 50 cells in 4 rats, MEC lesion, $n = 164$ fields from 153 cells in 6 rats) and during PSSFs (control, $n = 31$ fields from 31 cells of 4 rats, MEC lesion, $n = 73$ fields from 62 cells of 5 rats). For the entire session, the place fields of MEC-lesioned rats were larger, the spatial information scores were lower, and the peak firing rates were lower compared to those of control rats ($P = 1.2 \times 10^{-6}$, $P = 1.59 \times 10^{-11}$, and $P = 2.9 \times 10^{-4}$, Mann-Whitney *U* tests). After selecting for PSSFs, these properties did not differ between control and MEC-lesioned rats ($P = 0.13$, $P = 0.20$, and $P = 0.37$, Mann-Whitney *U* tests). Mean firing rates on the track did not differ between control and MEC-lesioned rats during the entire session nor during PSSFs ($P = 0.34$ and $P = 0.81$, Mann-Whitney *U* tests). Dot plots include all data points and the median. *** $P < 0.001$. (k) The number of runs within PSSFs, normalized to the number of runs within the session, was substantially less in MEC-lesioned compared to control rats ($P = 3.5 \times 10^{-7}$, Mann-Whitney *U* test).

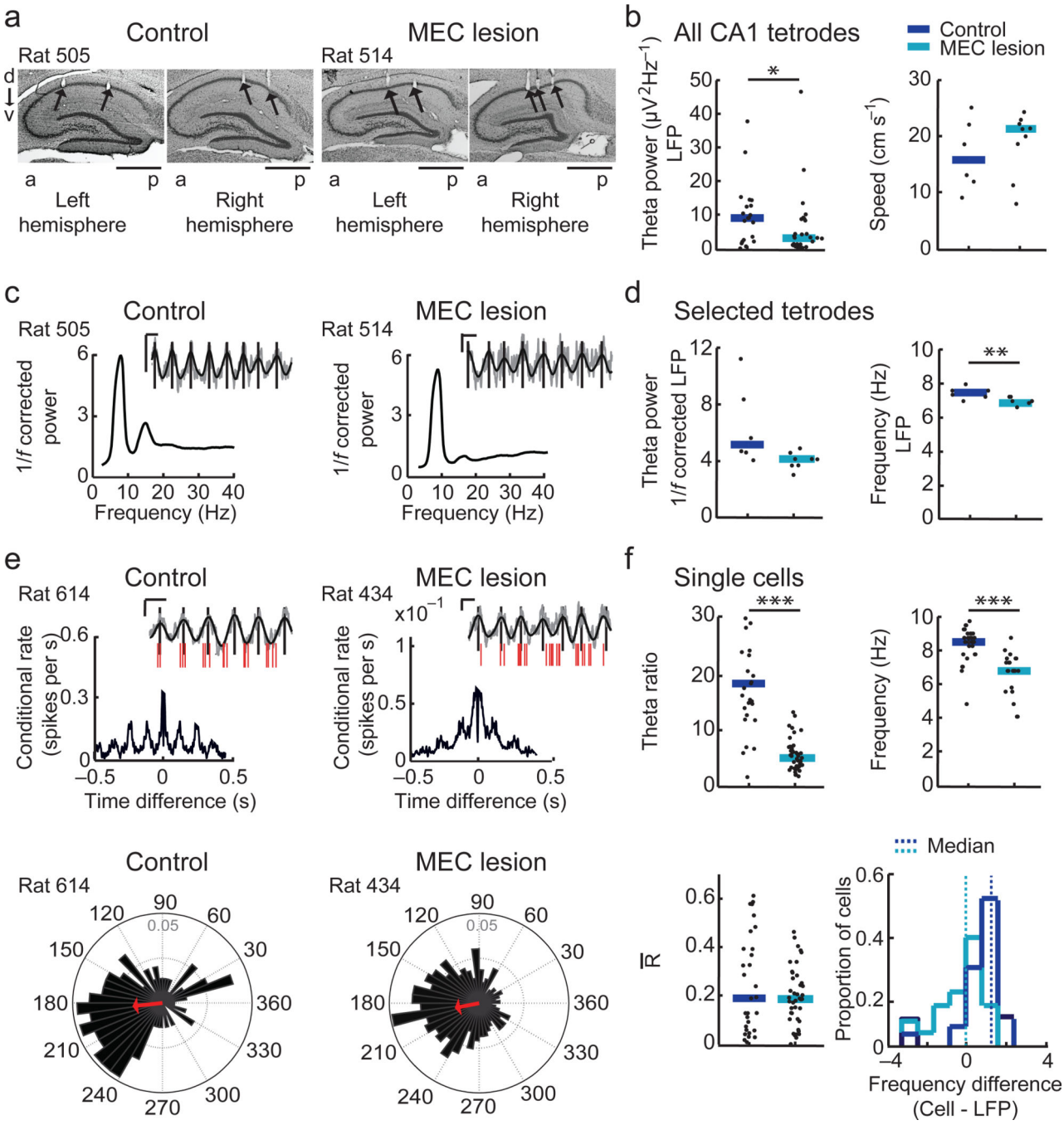

Figure 2. Theta rhythmicity is partially retained after MEC lesions

(**a**) Nissl-stained sagittal sections from the left and right dorsal hippocampus (d, dorsal; v, ventral; a, anterior; p, posterior). (**b**) On tetrodes in the CA1 cell layer, the theta power in the local field potential (LFP) was reduced by the MEC lesion (control, $n = 20$ tetrodes in 4 rats, MEC lesion, $n = 30$ tetrodes in 5 rats, $P = 0.015$, Mann-Whitney U tests) while the running speed was not different between groups ($P = 0.61$, Mann-Whitney U test). (**c**) To accurately calculate theta phase and frequency for each recording session, tetrodes for which the peak 1/f-corrected power in the theta band was > 3 times the baseline were selected. Spectrograms

for example selected tetrodes (see Supplementary Fig. 1 for spectrograms from all rats with PSSFs). Insets show raw (gray line) and filtered LFP traces (4–12 Hz, black line) during a single pass through a place field. Vertical lines, peak of each LFP theta cycle. Scale bars, 250 μV and 100 ms. (**d**) The 1/*f* corrected theta power of selected tetrodes did not differ (control, $n = 6$ sessions in 4 rats, MEC lesion, 9 sessions in 5 rats, $P = 0.066$, Mann-Whitney *U* test), while the theta frequency was reduced by the MEC lesion ($P = 0.0052$, Mann-Whitney *U* test). (**e**, top) Spike-time autocorrelograms of representative CA1 cells. Insets: spike times (red ticks) during a single pass through the cell's place field relative to the LFP theta signal (displayed as in **c**). (**e**, bottom) Phase distribution plots with the mean resultant vector ($\bar{R}$, red arrow) indicating the degree of phase locking to the LFP theta cycle for the example cells above. (**f**, top) The amplitude and frequency of the cells' theta modulation were reduced in MEC-lesioned compared to control rats (amplitude: control, $n = 30$ cells in 4 rats, MEC lesion, $n = 41$ cells in 5 rats; $P = 5.7 \times 10^{-10}$; frequency: control, $n = 29$ cells in 4 rats, MEC lesion, $n = 21$ cells in 4 rats, $P = 3.9 \times 10^{-6}$, Mann-Whitney *U* tests). Only theta modulated cells (theta ratio > 5) were included in the frequency analysis. Dot plots include individual data points and medians. * $P < 0.05$, ** $P < 0.01$, *** $P < 0.001$. (**f**, bottom left) Theta phase locking of CA1 cells, as assessed from the median length of $\bar{R}$ did not differ between cells from control and MEC-lesioned rats ($P = 0.57$, Mann-Whitney *U* test). (**f**, bottom right) Difference between the cells' and the LFP theta frequency. Control cells fired at a higher frequency than LFP theta ($P = 1.5 \times 10^{-5}$, sign test), while cells of MEC-lesioned rats fired without a consistent difference to LFP theta frequency ($P = 1.00$, sign test). The frequency difference was higher in control compared to MEC-lesioned rats ($P = 6.5 \times 10^{-5}$, Mann-Whitney *U* test).

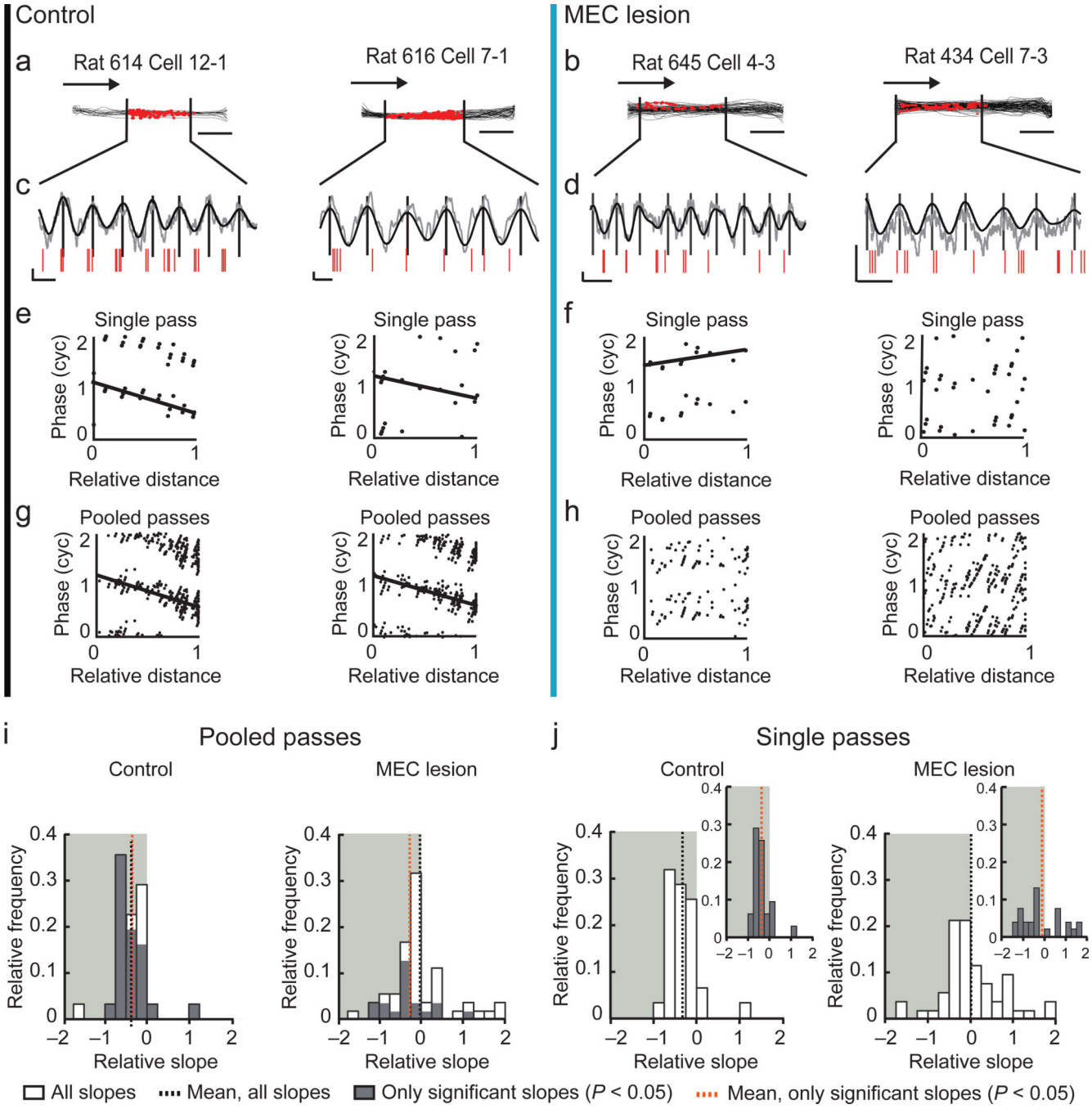

Figure 3. The medial entorhinal cortex is necessary for hippocampal phase precession

(**a**–**h**) Each column includes data from one example place field (control, black vertical line; MEC lesion, blue vertical line). (**a,b**) Trajectories (black lines) and spike locations (red dots) within the place field. Vertical lines delineate the place field boundaries. (**c,d**) Raw LFP trace (gray), filtered LFP trace (4–12 Hz, black), and spike times (red ticks) for a single pass through the place field. Vertical lines indicate the peak of each theta cycle. Scale bars, 250 μV and 100 ms. (**e**–**h**) The theta phase at which each spike occurred versus the relative distance that the rat traveled through the place field. For better visualization, the phase of

each spike is replotted in a second cycle in all phase-distance plots. A regression line (black) was added when the circular-linear correlation was significant ($P < 0.05$). (**i,j**) Distributions of the phase-distance slopes. Only fields defined during PSSFs were included. The shaded background highlights negative slopes. (**i**) For each field, the spikes from all passes were pooled before fitting the regression lines. Slopes were less than zero for control fields (all slopes: $n = 31$ in 4 rats, $P = 3.3 \times 10^{-5}$; only significant slopes: $n = 25$, $P = 6.2 \times 10^{-5}$, *t* tests) and, for fields from MEC-lesioned rats, not different from zero for all slopes ($n = 50$ in 5 rats, $P = 0.73$), but less than zero for only significant slopes ($n = 18$ fields, $P = 0.039$, *t* tests). Slopes also substantially differed between control and MEC-lesioned rats ($P = 0.0095$, *t* test). (**j**) Slopes that were first calculated for single passes through each field and then averaged per field. Insets: field-average of only significant single-pass slopes ($P < 0.05$, circular-linear correlation). Slopes were different from zero for control fields (all slopes: $n = 31$, $P = 2.6 \times 10^{-5}$; only significant slopes: $n = 25$ fields, $P = 0.00015$, *t* tests) but not for fields from MEC-lesioned rats (all slopes: $n = 50$ fields, $P = 0.90$; only significant slopes: $n = 27$ fields, $P = 0.53$, *t* tests), and differed between control and MEC-lesioned rats (all slopes: $P = 0.0062$, *t* test)

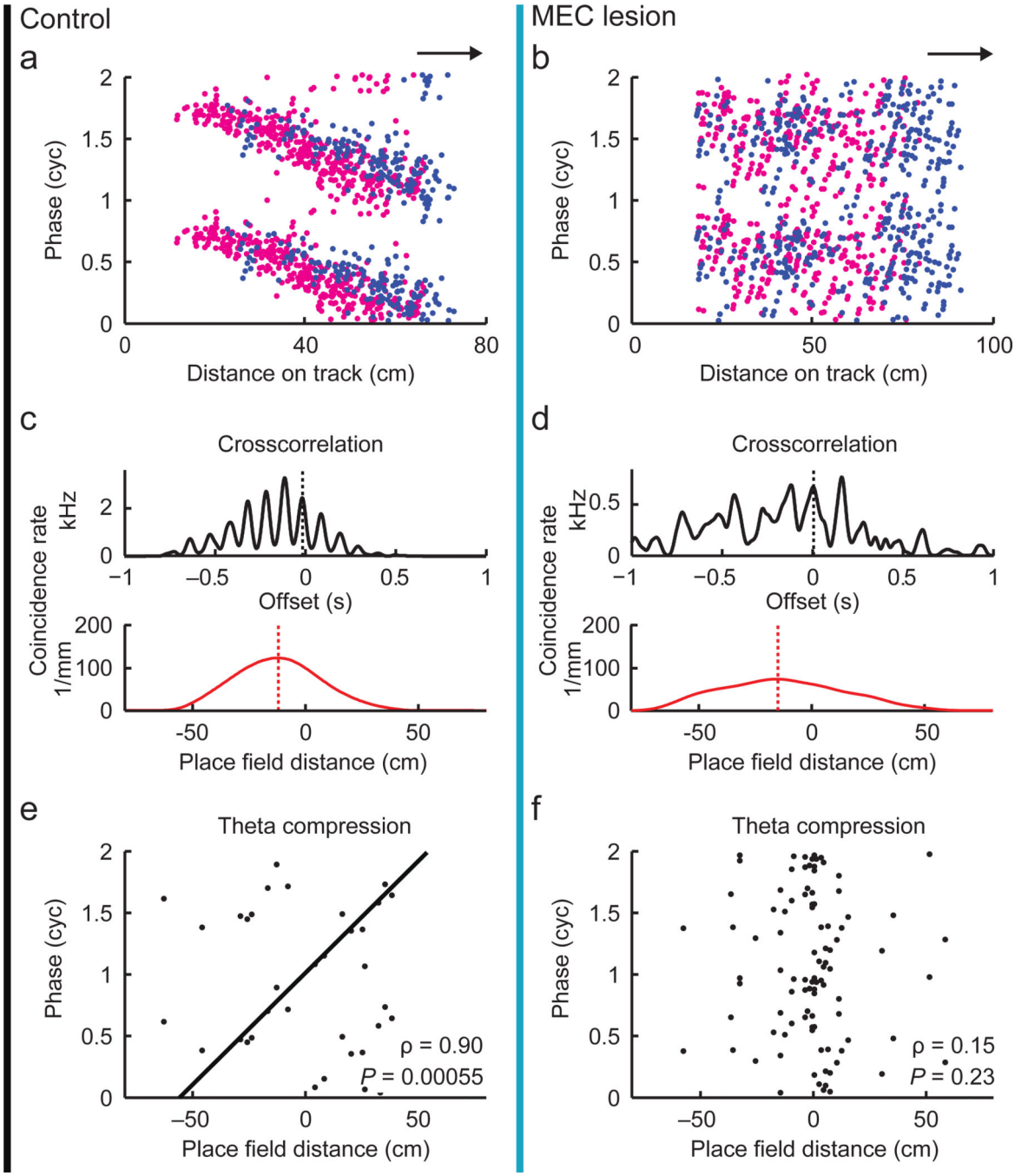

Figure 4. Spike timing between pairs of fields was disrupted in MEC-lesioned rats

(**a,b**) Example cell pairs with overlapping fields defined during PSSFs (control, black line; MEC lesion, blue line). Spikes of the two cells in a pair are in magenta and blue. Arrows indicate running direction. (**c,d**) Crosscorrelations between the two cells' spike trains (black) and the corresponding place fields (red) for the example pairs shown above. The black stippled line illustrates the theta phase offset (measured in Hilbert phase with respect to the theta band oscillations of the black correlation function). The red stippled line indicates the place field distance, defined as the shift of the maximum of the place field crosscorrelation

function. (**e,f**) Theta phase offset versus place field distance for all simultaneously recorded pairs of cells with overlapping fields (control, n = 18 pairs from 4 rats, MEC lesion, 63 pairs from 3 rats). Place field distance and theta offset exhibit a circular-linear correlation for control pairs, but not for pairs from MEC-lesioned rats.

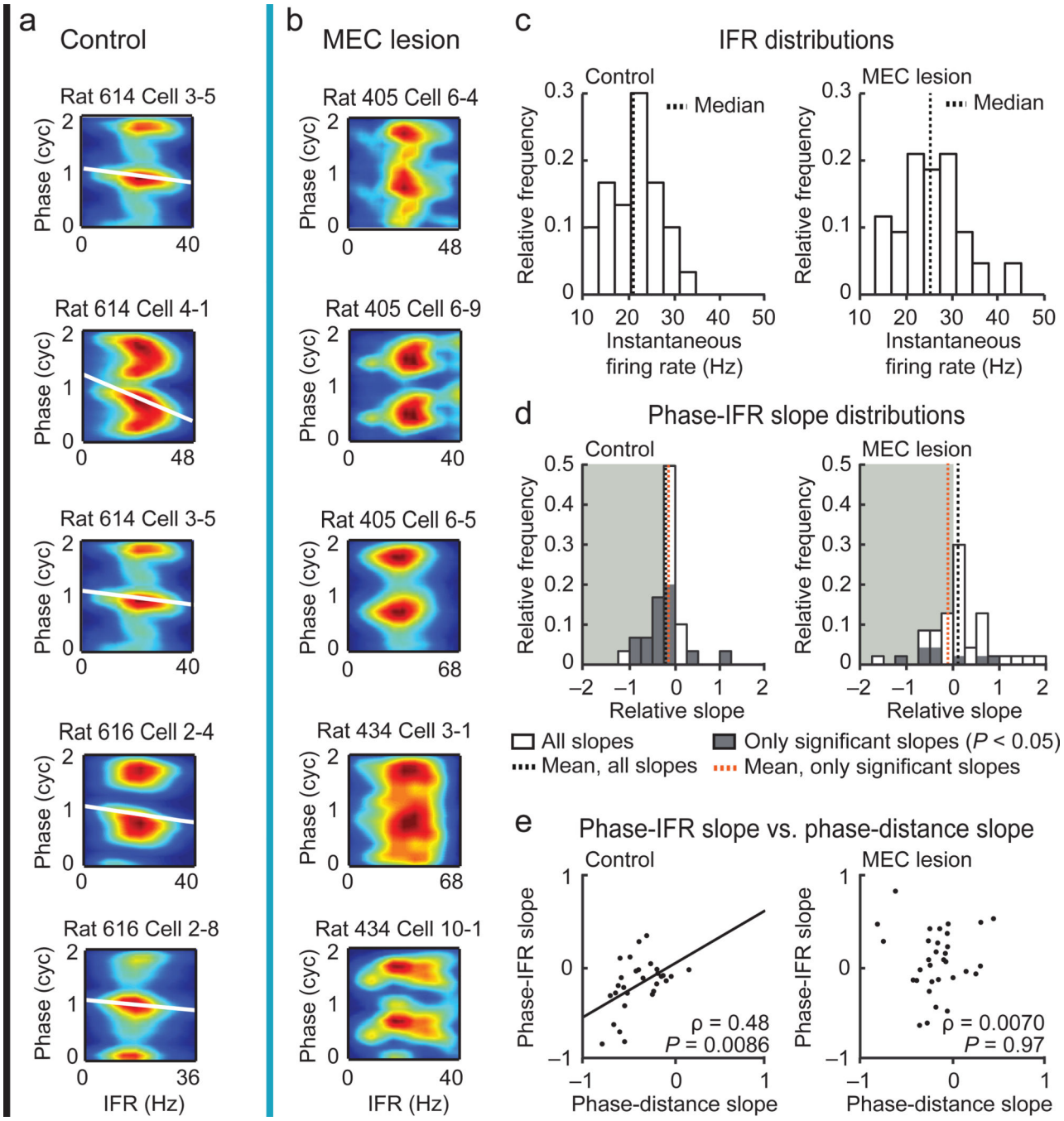

Figure 5. Instantaneous firing rate did not predict firing phase in MEC-lesioned rats

(**a,b**) Firing phase-instantaneous firing rate (IFR) spike density plots (blue to red, zero to maximum density) for example cells (control, black line; MEC lesion, blue line). For better visualization, the phase is replotted in a second cycle. For each cell, a regression line (white) is added when the circular-linear correlation between firing phase and IFR was significant ($P < 0.05$). (**c**) The average IFR per cell was higher in MEC-lesioned rats compared to controls ($n = 30$ cells in 4 control rats and 43 cells in 5 MEC-lesioned rats, $P = 0.0024$, Mann-Whitney U test), which excludes the possibility that the loss of phase-IFR correlation

can be explained by a smaller range of firing rates in the MEC lesion group. (**d**) Distributions of phase-IFR slopes. The shaded background highlights negative slopes. The mean slope was smaller than zero in control rats (all slopes, $P = 0.010$; only significant slopes, $P = 0.047$, *t* tests), not different from zero in MEC-lesioned rats (all slopes, $P = 0.55$; only significant slopes, $P = 0.36$, *t* tests), and less negative in MEC-lesioned rats than in control rats (all slopes, $P = 0.016$, *t* test). (**e**) The phase-IFR slope correlated with the phase-distance slope in control rats, while no such correlation was observed in MEC-lesioned rats (control, n = 29 fields in 4 rats, MEC lesion, 32 fields in 5 rats, includes only fields in which both slopes were between −1 and +1, Pearson's correlation).

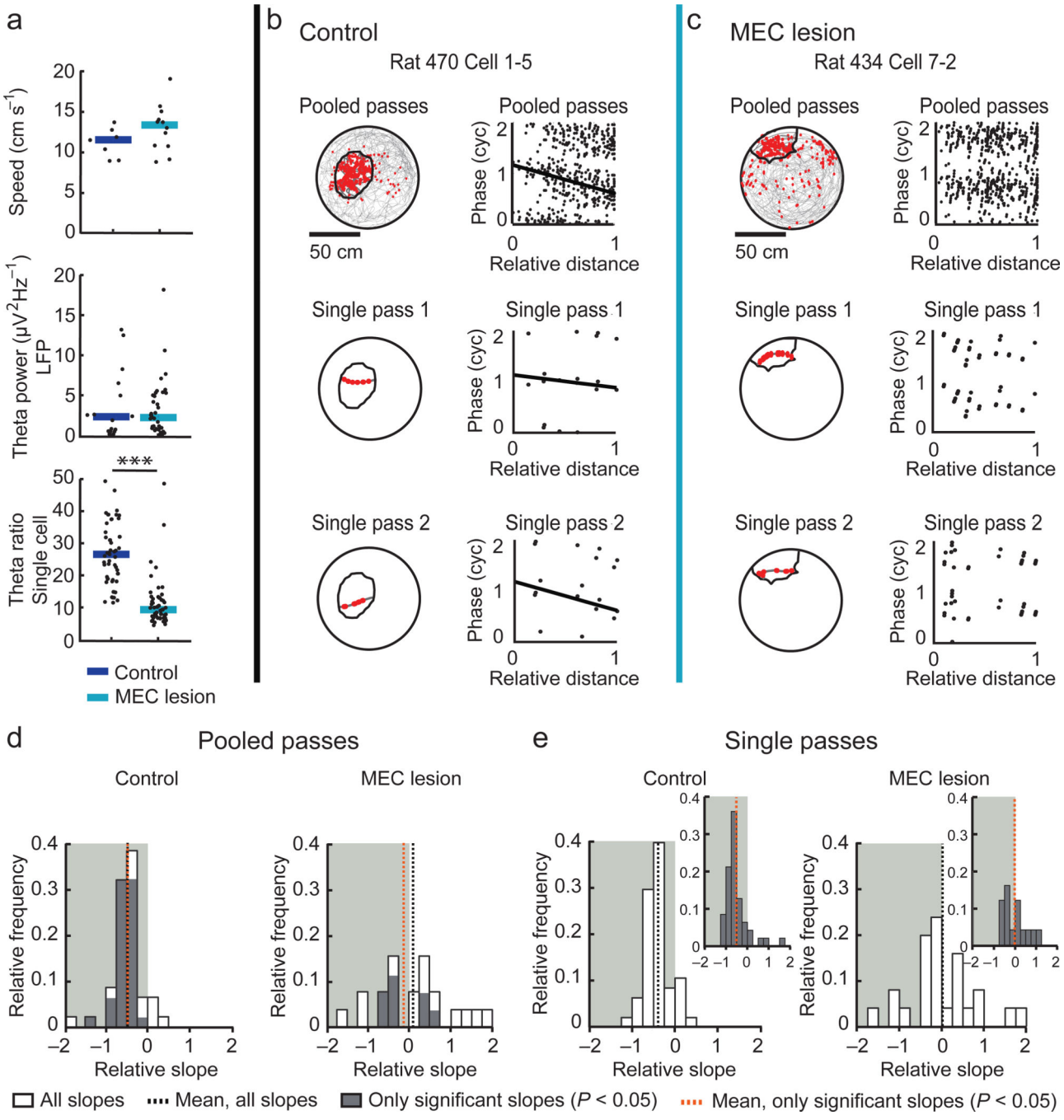

Figure 6. Phase precession was also diminished in the open field

Hippocampal CA1 cells were recorded during 10-min random foraging sessions, and cells with place fields < 0.25 m^2 were included in the analysis. (**a**) MEC-lesioned rats performed the task at a similar speed to control rats (top; control, n = 7 sessions in 3 rats, MEC lesion, n = 12 sessions in 4 rats, P = 0.12, Mann-Whitney U test). LFP theta power was not different (middle; control, n = 16 tetrodes in 3 rats, MEC lesion, n = 39 tetrodes in 4 rats, P = 0.76, Mann-Whitney U test), while the theta modulation of individual cells was reduced in MEC-lesioned rats compared to controls (bottom; control, n = 45 cells in 3 rats; MEC

lesion, $n = 24$ cells in 4 rats; $P = 4.4 \times 10^{-8}$, Mann-Whitney U test). (**b,c**) Spike patterns of example cells. (Left of each panel) Trajectories (gray line) with spike locations (red dots) and field boundaries (black line). The entire session is on top and two individual passes through the field are below. (Right of each panel) Phase-distance plots for the passes to the left. Regression lines (black) were added when the circular-linear correlation was significant ($P < 0.05$). (**d,e**) Distributions of the phase-distance slopes. In **d**, the spikes from all passes through the field were pooled before fitting the regression line. Slopes were different from zero for control fields (all slopes: $n = 46$ fields in 3 rats, $P = 6.6 \times 10^{-12}$; only significant slopes: $n = 35$ fields, $P = 1.4 \times 10^{-16}$, t tests), but not for fields from MEC-lesioned rats (all slopes: 21 fields in 4 rats, $P = 0.61$; only significant slopes: $n = 8$, $P = 0.39$, t tests) and differed between control and MEC-lesioned rats (all slopes: $P = 0.010$, t test). In **e**, slopes were first calculated for single passes through each field and then averaged per field. Insets: field-average of only significant single-pass slopes ($P < 0.05$, circular-linear correlation). Slopes differed from zero for control fields (all slopes: $n = 47$ in 3 rats, $P = 1.44 \times 10^{-12}$; only significant slopes: $n = 45$, $P = 2.8 \times 10^{-8}$, t tests), but not for fields from MEC-lesioned rats (all slopes: $n = 25$ in 4 rats, $P = 0.91$; only significant slopes: $n = 15$, $P = 0.89$, t tests), and were more negative in control compared to MEC-lesioned rats (all slopes: $P = 0.019$, t test). Dot plots include individual data points and medians. *** $P < 0.001$.

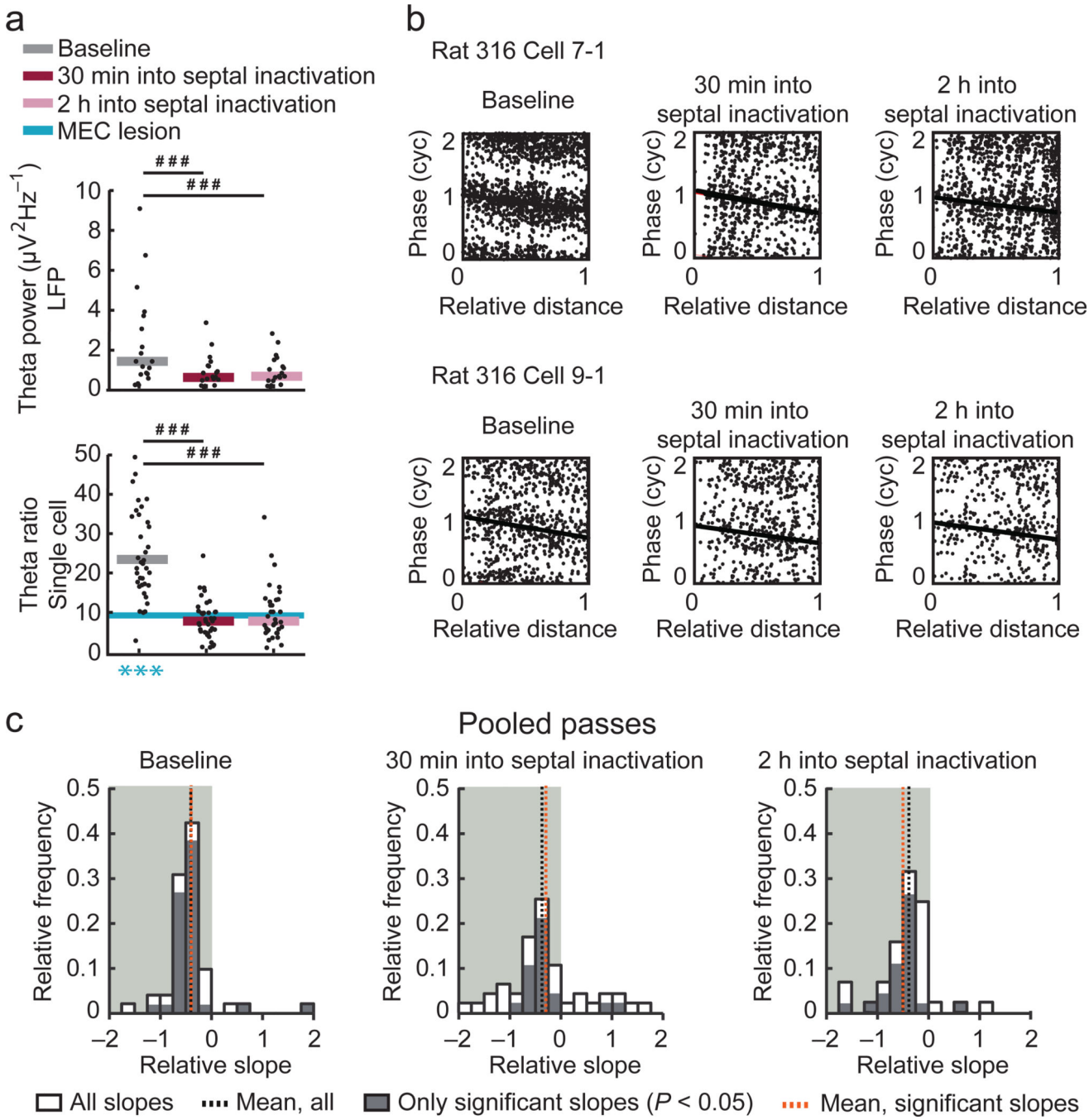

Figure 7. Substantially reduced LFP theta power and single-cell theta modulation did not preclude phase precession

The spike timing of hippocampal CA1 cells was analyzed for a 10-minute session before and for two sessions during inactivation of the septal area. (**a**) Hippocampal LFP theta power and the theta frequency modulation of individual hippocampal cells were substantially reduced between baseline and each of the two inactivation sessions (LFP power: $n = 19$ pairwise comparisons between tetrodes in 4 rats, $P = 0.00040$ and $P = 0.00040$; cells' theta modulation: $n = 39$ pairwise comparisons between cells in 4 rats, $P =$

1.1×10^{-6} and $n = 35$ in 4 rats, $P = 1.8 \times 10^{-5}$, Wilcoxon signed rank tests, Holm-Bonferroni corrected). Theta modulation was reduced to a similar extent during the inactivation as by the MEC lesion (blue line, median redrawn from Fig. 6a; baseline, 30 min into inactivation, and 2 h into inactivation vs. MEC lesion, $n = 41$, 39, 35, and 24 cells, $P = 1.9 \times 10^{-6}$, $P = 0.14$, and $P = 0.26$, Mann Whitney U tests, Holm-Bonferroni corrected). (**b**) Phase-distance plots for example fields from cells that were recorded before and during septal inactivation. For better visualization, the phase of each spike is replotted in a second cycle. Spike for each field were pooled, and regression lines (black) were added when the circular-linear correlation was significant ($P < 0.05$). (**c**) Distributions of phase-distance slopes. The phase-distance slopes were negative before inactivation (baseline, all slopes: $n = 51$ fields in 4 rats, $P = 2.0 \times 10^{-11}$, sign test; only significant slopes: $n = 39$ fields in 4 rats, $P = 2.8 \times 10^{-9}$, sign tests) and remained negative during the two inactivation sessions (all slopes: $n = 44$ and 42 fields in 4 rats, $P = 0.00039$ and $P = 5.6 \times 10^{-9}$; only significant slopes: $n = 20$ and 23 fields in 4 rats, $P = 0.00040$ and $P = 5.7 \times 10^{-6}$, sign test for the sessions 30 min and at 2 h into the inactivation, respectively). *** $P < 0.001$, compared to zero.### $P < 0.001$, baseline vs. inactivation sessions.

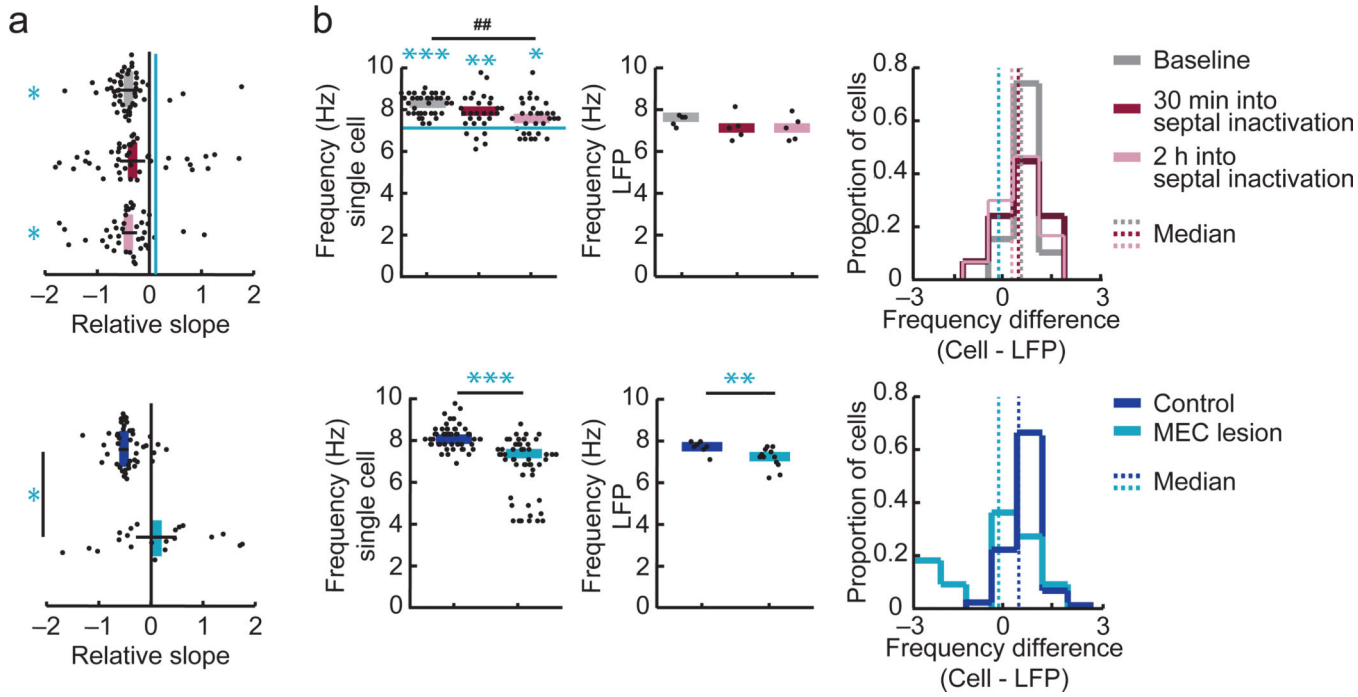

Figure 8. Phase precession was retained to a larger extent during septal inactivation than by the MEC lesion

(**a**) (Top) Phase-distance slopes were more negative during baseline (n = 51 fields in 4 rats) and during the session 2 h into the septal inactivation (n = 42 fields in 4 rats) compared to MEC-lesioned rats (blue line; n = 21 fields in 4 rats, P = 0.36 and P = 0.037, Mann-Whitney U tests, Holm-Bonferroni corrected). The difference between the MEC lesion group and the session 30 min into the septal inactivation session did not reach significance (n = 44 fields in 4 rats, P = 0.081, Mann-Whitney U test). (Bottom) Corresponding comparison between the MEC lesion and control group (data and statistics as in Fig. 6d). Dot plots include each field's slope and mean ± SEM. (**b**) The single cell but not the LFP oscillation frequency was reduced 2 h into the septal inactivation compared to baseline (P = 0.0015 and P = 0.56, respectively, Wilcoxon signed rank tests, Holm-Bonferroni corrected), and neither frequency was reduced 30 min into the septal inactivation (P = 0.16 and P = 0.56, Wilcoxon signed rank tests, Holm-Bonferroni corrected). The frequency difference was less than zero during baseline ($P = 2.8 \times 10^{-10}$, sign test) and remained different from zero during the two inactivation sessions (30 min into septal inactivation, P = 0.00033; 2 h into septal inactivation, P = 0.036, sign tests) and was not different from baseline during each of the inactivation sessions (P = 0.95 and P = 0.62, Wilcoxon signed rank tests). MEC lesions resulted in reduced theta frequency of single cells and of the LFP, but the single-cell frequency was reduced to a larger extent such that the frequency difference was no longer different from zero (control, $P = 9.43 \times 10^{-7}$, MEC lesion, P = 0.52, sign tests). In addition, there was a greater reduction in the frequency difference by MEC lesion than during baseline and during each of the two septal inactivation sessions (P = 0.00023, P = 0.0038 and P = 0.026, Mann-Whitney U tests, Holm-Bonferroni corrected). Only theta-modulated cells (theta ratio > 5; baseline, n = 40/41 in 4 rats, 30 min into septal inactivation, n = 31/39 in 4 rats, 2 h into septal inactivation, n = 30/35 in 4 rats, control, n = 45/45 in 4 rats, MEC

lesion, n = 23/24 cells in 4 rats) were used to calculate the frequency of the cells' firing. See Supplementary Tables 1, 3, and 4 for detailed statistics. ## $P < 0.01$, baseline vs. septal inactivation sessions. * $P < 0.05$, ** $P < 0.01$, *** $P < 0.001$, MEC lesion group vs. baseline, vs. 30 min into septal inactivation, and vs. 2 h into septal inactivation, and vs. control group.